NASA TECHNICAL NOTE

NASA TN D-2226

NASA TN D-2226

INVESTIGATION OF PLASMA AFTERGLOWS WITH APPLICATION IN NITROGEN

by K. C. Stotz

Prepared under Grant No. NsG-48-60 *by*
RENNSELAER POLYTECHNIC INSTITUTE
Troy, New York
for

NATIONAL AERONAUTICS AND SPACE ADMINISTRATION • WASHINGTON, D. C. • NOVEMBER 1963

TECHNICAL NOTE D-2226

INVESTIGATION OF PLASMA AFTERGLOWS WITH APPLICATION IN NITROGEN

By K. C. Stotz

Prepared under Grant No. NsG-48-60 by
RENNSELAER POLYTECHNIC INSTITUTE
Troy, New York

for

NATIONAL AERONAUTICS AND SPACE ADMINISTRATION

TABLE OF CONTENTS

LIST OF FIGURES

PART I.

INTRODUCTION AND HISTORICAL REVIEW

The importance of understanding the ionized state of gases has become realized in recent years with the enthusiastic attempt to solve such problems as nuclear fusion, magnetohydrodynamic generation of electricity, propagation of radiowaves in the ionosphere, and ionic engine space propulsion. Phenomena associated with gaseous plasma are in general complicated by the presence of a large number of particles and the simultaneous occurrence of various events. The study of isolated basic processes may therefore lead to a basic understanding of these phenomena.

Since the advent of the microwave method for detecting electron densities in ionized gases by S. C. Brown[20] in 1948, the study of the basic electron loss processes in afterglows (the time following the removal of the ionizing energy source) has received considerable attention. Prior to the development of microwave techniques, electron densities were measured mostly by Langmuir probes, which are discussed in detail in various texts on plasma electronics, e.g., Loeb[36]. Since the electron collection by the probe disturbs the plasma to some extent, it is difficult to interpret probe measurements. Probe measurements are extremely difficult to make in rapidly changing plasma situations, so their main contributions to date are results of studies in steady state gas discharges.

By employing the microwave technique, one is able to measure rapid changes in electron density; thus the basic electron loss processes may be studied in the afterglow. The removal of the energy source greatly simplifies the experimental conditions. Since highly sensitive microwave detection devices are available, signals of extremely low amplitude may be used. Measurements may therefore be made with probing signals which may be considered to have a negligible effect on the phenomena to be studied.

Initial studies employing microwave techniques were concentrated on determinations of electron losses by recombination and diffusion in the inert gases[14,15,33], especially helium. It was at first assumed that the afterglow contained only atomic ions, electrons, and neutral particles, but results of determinations of the recombination coefficient in helium were approximately a factor of 10^4 higher than expected. Bates[8] proposed a theory on dissociative recombination of the molecular ion, He_2^+, which would explain the higher recombination rate, and the presence of the molecular ion in the afterglow was confirmed with a mass spectrometer study by Phelps and Brown[48]. As a result of this work, it was realized that afterglow studies by the microwave technique must be supplemented by additional experimental procedures in order to separate properly the various events which are taking place.

Microwave techniques may basically be divided into two groups: 1) the cavity method, originally introduced by S. C. Brown, in which the electron density and collision frequency are related to the shift in the resonant frequency of a microwave cavity containing the plasma and the absorption loss or "Q" of the cavity and 2) the transmission method, introduced by Anderson and Goldstein[2], in which the microwave signal is passed through the plasma and the electron density and collision frequency are related to the phase shift and attenuation of the microwave signal.

Various authors have reported results of measurements in nitrogen. In the 1930's, Mitchell and Ridler[46] and Tyndall and Pearce[53] used a drift tube to measure the mobilities of various gases in nitrogen. The first results determined by the microwave technique (cavity) were reported by Biondi and Brown[15] in 1949. Since that time, other measurements employing the microwave technique were reported by: Anderson and Goldstein[3] (1956, transmission); Bialecki and Dougal[13] (1958, transmission); Faire and Champion[28] (1959, cavity); Formato and Gilardini[29] (1960, transmission); and Kasner, Rogers and Biondi[34] (1961, cavity).

Measurements of electron loss coefficients and cross-sections for momentum transfer in nitrogen by the two microwave methods have

shown different results. Formato and Gilardini[29] have proposed that the measurements by the transmission method might have been carried out early in the afterglow before the temperature had relaxed to room temperature, although the measurements were assumed to be carried out in a room temperature isothermal gas. Precise measurements of electron temperature in the afterglow have not been made to this date, but there is no question of the necessity for such measurements in order to completely describe the afterglow.

In this report the nitrogen afterglow has been studied using the microwave transmission technique as the basic diagnostic tool. A concerted effort has been made to simplify the experimental conditions in order to remove some of the questionable assumptions made in previous transmission method experiments. A plasma cell has been developed which consists essentially of a piece of standard waveguide, so that a simple rectangular geometry with well-defined boundaries is obtained for the microwave-plasma interaction. A microwave bridge circuit has been developed so that simultaneous measurements of the attenuation and phase shift of the microwave signal passing through the plasma are obtained. The bridge is calibrated directly by a precision attenuator and phase shifter in the microwave circuit.

In addition to the microwave measurements, a newly developed gated microwave radiometer was used to measure the electron temperature variation in the afterglow. A spectrographic study of the afterglow was made and a method for studying the light intensity as a function of time is discussed. By this variety of techniques, previous results obtained by using the microwave transmission method alone are shown to be in error and results of the present experiment are shown to be in agreement with cavity measurements. Although some question as to the actual recombination mechanism in the nitrogen afterglow still exists, the possibilities are discussed and narrowed as much as possible.

PART II.

THEORY

A. Conductivity of a Plasma at Microwave Frequencies

Considerable work has been done on the theory of the conductivity of plasmas at microwave frequencies in the past ten years[25,30,38]. The permittivity of the medium is usually taken as that of free space and the plasma is then completely described by the conductivity parameter. Conductivity is defined as the ratio of the current density to the electric field intensity producing it, where both quantities are assumed to have the time variation $e^{j\omega t}$ where ω is the angular frequency in radians/second.

The equation of motion for the electrons is written[17]

$$m \frac{d\bar{v}}{dt} + m\bar{v}\nu_m = q\bar{E} \qquad (1)$$

where the second term represents a damping term, and closer inspection would reveal that the effective collision frequency for momentum transfer ν_m has been taken independent of velocity. $\bar{E}$ is the electric field of the probing microwave signal and q the electron charge. It is advantageous to discuss the derivation of equation 1 to indicate the assumptions that have been made.

The model used is close to that of a free electron gas. It is assumed that the heavier ions do not respond to the electric field of the probing microwave signal. The gaseous plasma is composed of electrons, positive ions and neutral molecules (in the case of an electro-negative gas, negative ions would also be present). A distribution function would exist for each species of the gas and a Boltzmann equation is written for each of the species. The equations are normally coupled through the collision terms. Consider the Boltzmann equation for electrons

$$\frac{\partial f_e}{\partial t} + \bar{v} \cdot \frac{\partial f_e}{\partial \bar{r}} + \bar{a}_e \cdot \frac{\partial f_e}{\partial \bar{v}} = C_{ee} + C_{eI} + C_{eN} \qquad (2)$$

where f_e denotes the distribution function for electrons. The terms on the right hand side represent non-explicitly the rate of change of the electron distribution function due to collisions where C_{ee} is the rate of change of the electron distribution function due to collisions among electrons, C_{eI} due to collisions between electrons and ions, and C_{eN} between electrons and neutral molecules. A great simplification is obtained if the gas is weakly ionized so that $n_e \ll N$ where n_e is the electron density and N is the neutral molecule density. It is assumed throughout that the plasma is charge neutral, so that the electron density is approximately equal to the ion density, n_I. In the weakly ionized case, the model assumed is that the electrons find themselves in a "sea" of neutrals, so that the electron-electron collisions and the electron-ion collisions are negligible in comparison with the electron-neutral molecule collisions. Delcroix[24] somewhat arbitrarily defines a weakly ionized plasma as one where

$$\frac{n_e}{n_e + N} \ll 10^{-4} \qquad (3)$$

At room temperature and 1 mm of mercury pressure, the molecular density is approximately 3×10^{16} particles per cm^3. Since this is in the range of pressures used in the experiments and the maximum electron density used in obtaining data was approximately 10^{12} electrons per cm^3, the above inequality holds true. It especially holds true in the late afterglow when electron loss processes are determined, the electron densities here being in the order of 10^9 - 10^{10} electrons per cubic centimeter.

The equation of motion 1 is obtained by taking the so-called second moment of the Boltzmann equation (multiplying each term by the momentum mv and integrating over velocity space). The term involving the pressure tensor has been omitted, since motion due to pressure gradients is negligible with respect to motion caused by the electric field in computing the conductivity. The collision term, which is normally written $\partial f / \partial t \,|_c$, may be expressed as $-f \nu_m$ where ν_m is the collision frequency for momentum transfer. This assumes that

the frequency of the microwave field is sufficiently high so that no appreciable change of electron energy or density occurs within a single cycle. The distribution function f is then independent of time. Strictly speaking, equation 1 should be written

$$\frac{\partial}{\partial t}(m\langle\bar{v}\rangle) + m\nu_m\langle\bar{v}\rangle = m\langle\bar{a}\rangle \tag{4}$$

where the symbol $\langle\ \rangle$ above represents that the quantity has been averaged over velocity space. These brackets will be dropped in the following discussion. The collision frequency is physically a frequency of collision for momentum transfer and has been assumed independent of velocity. The acceleration term in equation 4 is a result of the electric field intensity, $\bar{E}$, of the probing microwave signal, and is written as

$$\bar{a} = \frac{q\bar{E}}{m} = \frac{q\bar{E}_o e^{j\omega t}}{m} \tag{5}$$

The solution of equation 4 becomes

$$\bar{v} = \frac{q\bar{E}}{m(\nu_m + j\omega)} \tag{6}$$

and since the current density $\bar{J}$ is equal to the charge, q, times the particle flow $n_e\bar{v}$

$$\bar{J} = \frac{n_e q^2 \bar{E}}{m(\nu_m + j\omega)} \tag{7}$$

The conductivity has been defined as the ratio of the current density and electric field intensity so that the complex conductivity, σ , may be obtained from equation 7.

$$\sigma = \frac{n_e q^2}{m(\nu_m + j\omega)} \tag{8}$$

This may be separated into real and imaginary parts, σ_r and σ_i,

where

$$\sigma_r = \frac{n_e q^2 \nu_m}{m(\nu_m^2 + \omega^2)} \tag{9}$$

and

$$\sigma_i = \frac{-n_e q^2 \omega}{m(\nu_m^2 + \omega^2)} \tag{10}$$

It is interesting to note here that in the absence of collisions ($\nu_m = 0$), the conductivity is purely imaginary and the model of the free electron gas is obtained.

The assumptions made in deriving the conductivity are valid except for the questionable assumption that the collision frequency is independent of velocity. The form indicated in equation 8 is in wide use, but in situations where collisions are important, e.g., in obtaining collision cross-sections, equation 8 must be taken as a first approximation. As it turns out, in the late afterglow at low pressures, the effect of collisions is negligible and electron loss process coefficients obtained after using equation 8 are valid.

B. Electron Losses in a Decaying Plasma

1. Introduction

The electrons formed in a gas discharge will disappear by three basic processes, when the source is removed. First, the electrons will recombine with positive ions. This process will be called volume recombination, or simply recombination, in the ensuing discussion. Secondly, the electrons will diffuse to the wall and they will disappear by "wall recombination". The third process is only important in the case of electro-negative gases, and that is the attachment of electrons to neutral molecules forming negative ions.

The type of diffusion encountered is ambipolar. The meaning of this term will be explained in the next section. The loss mechanisms are first discussed singly as though only one mechanism were taking

place at a time. After that the more difficult problem of combinations of loss mechanisms is discussed.

2. Ambipolar Diffusion

a. Positive ion-electron. Assume that the mean free path is much smaller than the dimensions of the container. Then normal diffusion of particles occurs as a result of a density gradient and is characterized by

$$\bar{\Gamma} = -D \nabla n \tag{11}$$

where $\bar{\Gamma}$ is the particle flux or flow and is equal to the product $n\bar{v}$, and D is the diffusion coefficient and has the dimensions of area/time. Electrons and ions recombine readily at the walls of the container, since the molecules or atoms of the wall material are available as third bodies to take up the liberated energy. The density of charged particles is thus essentially zero at the walls. This results in a density gradient and electrons and positive ions will diffuse to the wall. Because of the difference in masses, the electrons would diffuse faster than the positive ions. This phenomenon leads to a charge separation resulting in a space charge field, which is written as $\bar{E}_s$. We must therefore conclude that the diffusion of the electrons is retarded by the space charge field, so that both types of particles diffuse at the same rate. The simultaneous diffusion of both species may be characterized by an ambipolar diffusion coefficient, D_a, which may be found as a function of the diffusion coefficients and mobilities of the electrons and positive ions. On the assumption that the charge carriers consist of electrons and one type of positive ion, modified flow equations (equation 11) may be written as follows:

$$\bar{\Gamma}_e = -D_e \nabla n_e - n_e \mu_e \bar{E}_s$$

$$\bar{\Gamma}_+ = -D_+ \nabla n_+ + n_+ \mu_+ \bar{E}_s \tag{12}$$

where μ is the mobility (velocity per unit field). The second term on the right hand side describes the flow due to the space charge field $\bar{E}_s$. The densities of the electrons and ions are n_e and n_+ respectively. The basic assumption of a charge neutral plasma ($n_e = n_+$) and the assumption of equal flow rates lead to the property:

$$\bar{\Gamma}_+ = \bar{\Gamma}_e = \bar{\Gamma} \tag{13}$$

The space charge field and $\bar{\Gamma}$ may be found from equations 12 with the result

$$\bar{E}_s = - \frac{D_e - D_+}{\mu_e + \mu_+} \frac{\nabla n}{n} \tag{14}$$

where $\nabla n/n$ may refer to either electron densities or ion densities and

$$\bar{\Gamma} = - \frac{(\mu_e D_+ + \mu_+ D_e)}{(\mu_e + \mu_+)} \nabla n \tag{15}$$

Comparison of equations 11 and 15 shows that the ambipolar diffusion coefficient is

$$D_a = \frac{\mu_e D_+ + \mu_+ D_e}{\mu_e + \mu_+} \tag{16}$$

This expression may be simplified if the distribution function of both the electrons and positive ions is Maxwellian. In such a situation, the mobilities and diffusion coefficients are related by the Einstein relations[4]

$$\frac{\mu_+}{D_+} = \frac{q}{kT_g} \qquad \frac{\mu_e}{D_e} = \frac{q}{kT_e} \tag{17}$$

where k is the Boltzmann constant and q is the absolute value of the charge on an electron. The ion temperature will be essentially equal to the neutral gas temperature and has been written as T_g. With the

knowledge that the electron mobility is much larger than the ion mobility, the ambipolar diffusion coefficient becomes

$$D_a \approx D_+ \left[1 + \frac{T_e}{T_g}\right] \tag{18}$$

and in the case of an isothermal plasma where the electron temperature is also equal to the neutral gas temperature

$$D_a \approx 2D_+ = 2\mu_+ \frac{kT_g}{q} \tag{19}$$

It is seen, then, that if certain conditions are fulfilled, obtaining the ambipolar diffusion coefficient leads to knowledge of the positive ion diffusion coefficient and the mobility of the ion.

b. Electro-negative gases. Since gases composing the atmosphere are of special interest, it would be assumed that considerable work would be published on properties of oxygen. Neutral oxygen molecules have an affinity for electrons, thus forming negative ions. It is difficult to interpret measurements in such an electro-negative gas; thus, only preliminary results have been published to date.

For the study of ambipolar diffusion in an electro-negative gas, assume that the charge carriers consist of one type of positive ion of density n_+, one type of negative ion of density n_-, and electrons with density n_e.

The flow equations in this case become

$$\begin{aligned} \bar{\Gamma}_e &= -D_e \nabla n_e - n_e \mu_e \bar{E}_s \\ \bar{\Gamma}_+ &= -D_+ \nabla n_+ + n_+ \mu_+ \bar{E}_s \\ \bar{\Gamma}_- &= -D_- \nabla n_- - n_- \mu_- \bar{E}_s \end{aligned} \tag{20}$$

The neutrality condition of the plasma requires that

$$n_+ = n_e + n_-$$

and

$$\bar{\Gamma}_+ = \bar{\Gamma}_e + \bar{\Gamma}_- \tag{21}$$

It is assumed that the diffusion has been in effect long enough so that the spatial distribution of carriers is characterized by the fundamental diffusion mode. More will be said about this later, but in effect the assumption required is that the spatial distribution satisfying the breakdown mechanism has disappeared and has been replaced by one which satisfies the diffusion of the particles. If this condition is satisfied,

$$\frac{\nabla n_e}{n_e} = \frac{\nabla n_+}{n_+} = \frac{\nabla n_-}{n_-} \tag{22}$$

Under these conditions, equations 20 may be solved for the space charge field,

$$\bar{E}_s = - \frac{D_e n_e + D_- n_- - D_+ n_+}{n_+ \mu_+ + n_e \mu_e + n_- \mu_-} \quad \frac{\nabla n}{n} \tag{23}$$

in which the last factor in n may be replaced by any one of the three factors in equation 22.

If the flow equations are now written in terms of an ambipolar diffusion coefficient which accounts for the space charge effect:

$$\begin{aligned} \bar{\Gamma}_e &= -D_{ae} \nabla n_e \\ \bar{\Gamma}_+ &= -D_{a+} \nabla n_+ \\ \bar{\Gamma}_- &= -D_{a-} \nabla n_- \end{aligned} \tag{24}$$

The ambipolar diffusion coefficients may be found to be

$$\begin{aligned} D_{ae} &= \frac{(1+a)\left(\mu_e D_+ + \mu_+ D_e\right) + a\left(\mu_- D_e - \mu_e D_-\right)}{\mu_e + a\mu_- + (1+a)\mu_+} \\ D_{a-} &= \frac{(1+a)\left(\mu_+ D_- + \mu_- D_+\right) - \left(\mu_- D_e - \mu_e D_-\right)}{\mu_e + a\mu_- + (1+a)\mu_+} \\ D_{a+} &= \frac{\left(\mu_e D_+ + \mu_+ D_e\right) + \left(\mu_+ D_- + \mu_- D_+\right) a}{\mu_e + a\mu_- + (1+a)\mu_+} \end{aligned} \tag{25}$$

where $a = \frac{n_-}{n_e}$ or $(1 + a) = \frac{n_+}{n_e}$

In this case the ambipolar diffusion coefficients are different for each type of charge carrier and are dependent on the relative concentrations of the various densities. Note that if the negative ion density disappears ($n_- = a = 0$), then $D_{a+} = D_{ae}$ and these quantities are equal to the ambipolar diffusion coefficient found in the previous section.

These formidable expressions may be simplified, provided that the negative ion density is not large compared to the electron density. The mobility of the electron is larger than the mobilities of the massive positive and negative ions, so that the denominators of equation 25 may be written as approximately μ_e, provided that "a", which is the ratio n_-/n_e, is not too large. It is not difficult to realize this situtation in practice. Under this condition and using the Einstein relations (equation 17), the expressions 25 become

$$\begin{aligned} D_{ae} &= (1 + a)\, D_+ \left[1 + \frac{T_e}{T_g}\right] + aD_- \left[\frac{T_e}{T_g} - 1\right] \\ D_{a-} &= 2(1 + a)\, \frac{D_+ D_-}{D_e} - D_- \left[\frac{T_e}{T_g} - 1\right] \\ D_{a+} &= \left[1 + \frac{T_e}{T_g}\right] D_+ \end{aligned} \tag{26}$$

For an isothermal plasma ($T_e = T_g$), these expressions reduce further to

$$\begin{aligned} D_{ae} &= 2\,(1 + a)\, D_+ \\ D_{a-} &= 2\,(1 + a)\, \frac{D_+ D_-}{D_e} \\ D_{a+} &= 2\, D_+ \end{aligned} \tag{27}$$

It is seen in equations 27 that the ambipolar diffusion

coefficient of the positive ions is little affected by the presence of the negative ions in an isothermal plasma. The ambipolar diffusion of the electrons is increased by the ratio of the densities of the positive ions and electrons. D_{a-} is smaller than either D_{a+} or D_{ae}, since the ratio D_-/D_e is less than unity. In the absence of negative ions ($a = 0$), the result of the previous section is obtained with $D_{ae} = D_{a+} = 2D_+$. It must be remembered that the assumption has been made that the number density of the negative ions is not too large with respect to the density of electrons. In a situtation where this is not true, the more general expressions 25 would have to be used.

3. Electron Loss by Diffusion

The flow equation 11 is written with a free diffusion coefficient or ambipolar diffusion coefficient, depending on the particular experimental situation. Allis[4] has discussed the requirements in some detail. As might be expected, the diffusion will be ambipolar, provided the characteristic Debye shielding length is less than the dimensions of the vessel. The Debye length (rationalized MKS units are used) is given by

$$\ell_D = \sqrt{\frac{\epsilon_o kT}{n_e q^2}} \tag{28}$$

At room temperature and at an electron density of 10^8 per cubic centimeter, which is lower than the minimum detectable density in the experiments, the Debye length is less than a millimeter. This is much smaller than the dimensions of the vessel, so ambipolar diffusion is expected.

The continuity equation, which is obtainable from the first moment of the Boltzmann equation, is

$$\frac{\partial n}{\partial t} + \nabla \cdot \bar{\Gamma} = 0 \tag{29}$$

Inserting the equation of flow in terms of the ambipolar diffusion coefficient leads to the equation describing the time and spatial variation of the density.

$$\frac{\partial n}{\partial t} = D_a \nabla^2 n \tag{30}$$

It is assumed here that one type of positive ion and electrons are present and that $n_e = n_+ = n$. D_a then is given by equation 16. Equation 30 is easily solved, when the density is subject to simple boundary conditions, by a separation of variables technique. Two specific problems of interest will be worked out-- first, diffusion in a rectangular box and secondly, diffusion in a right circular cylinder.

The plasma cell in the experimental arrangement consists of a length of rectangular X-band waveguide. With a coordinate system in such a geometry as indicated in Figure 1, the solution to equation 30 is

$$n(x,y,z,t) = \sum_{k,\ell,m=1}^{\infty} K_{k,\ell,m} \exp\left[-\frac{D_a t}{\Lambda_{k,\ell,m}^2}\right] \sin\left(\frac{k\pi x}{a}\right)\sin\left(\frac{\ell\pi y}{b}\right)\sin\left(\frac{m\pi z}{c}\right) \tag{31}$$

where $\frac{1}{\Lambda_{k,\ell,m}^2} = \left(\frac{k\pi}{a}\right)^2 + \left(\frac{\ell\pi}{b}\right)^2 + \left(\frac{m\pi}{c}\right)^2$

$\Lambda_{k,\ell,m}$ is known as the characteristic diffusion length. a, b, and c are the dimensions of the rectangular vessel. The boundary conditions are that the electron density is zero at the walls because of wall recombination.

The coefficients $K_{k,\ell,m}$ are the Fourier coefficients; they depend on the initial electron density distribution and are given by

$$K_{k,\ell,m} = \frac{8}{abc} \int_0^c \int_0^b \int_0^a n(x,y,z,0)\sin\left(\frac{k\pi x}{a}\right)\sin\left(\frac{\ell\pi y}{b}\right)\sin\left(\frac{m\pi z}{c}\right) dx\, dy\, dz \tag{32}$$

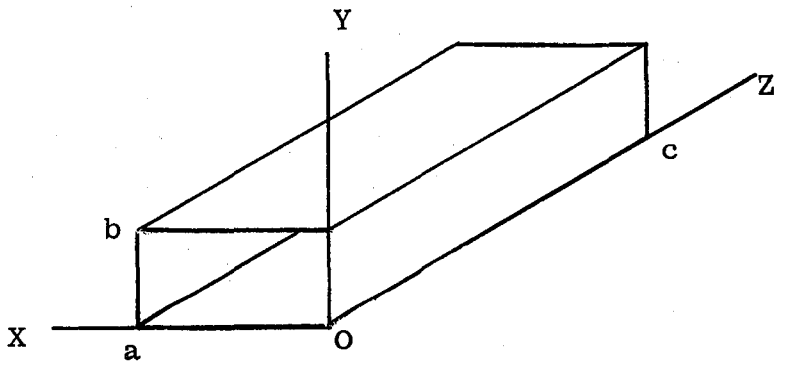

Fig. 1. Rectangular geometry for diffusion problem.

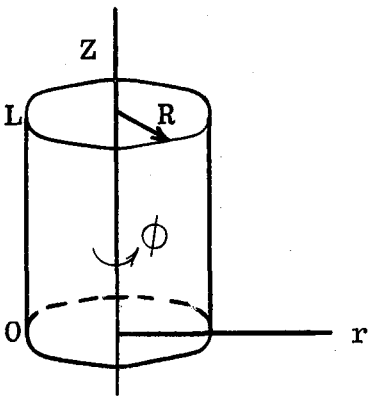

Fig. 2. Cylindrical geometry for diffusion problem.

It is noticed in equation 31 that if one waits long enough, the fundamental diffusion mode (with $k = \ell = m = 1$) will predominate and a semilogarithmic plot of n vs. t will be a straight line. The slope of the plot will give the ambipolar diffusion coefficient, D_a, since $\Lambda_{1,1,1}$ depends on the dimensions in a known fashion.

Another specific problem of interest is diffusion in a right circular cylinder. This problem has application in glass tube vessels and in cylindrical cavities. Assume the coordinate system origin to be at the bottom center of the cylinder as shown in Figure 2, and axial symmetry for the density function. The solution of equation 30 is then

$$n(r,z,t) = \sum_{k,\ell=1}^{\infty} K_{k,\ell} \exp\left[-\frac{D_a t}{\Lambda_{k,\ell}^2}\right] J_o(\lambda_{kR}\frac{r}{R})\sin(\frac{\ell\pi}{L}z) \qquad (33)$$

where $$\frac{1}{\Lambda_{k,\ell}^2} = (\frac{\lambda k}{R})^2 + (\frac{\ell\pi}{L})^2$$

λ_k is the kth root of the zero order Bessel function J_o. The Fourier-Bessel coefficient, $K_{k,\ell}$, may be found from the initial electron density distribution $n(r,z,o)$ and is given by

$$K_{k'\ell} = \frac{4}{L\left[RJ_1(\lambda_k)\right]^2} \int_o^R \int_o^L n(r,z,o) r J_o(\lambda_{kR}\frac{r}{R})\sin(\frac{\ell\pi}{L}z)\, dz\, dr \qquad (34)$$

As in the case of rectangular boxes, the ambipolar diffusion coefficient may be found from the slope of the semilogarithmic plot

of the electron density vs. time when the fundamental diffusion mode is predominant.

4. Electron Loss by Recombination

Recombination between positive ions and electrons may take place in a variety of ways, i.e., radiative, di-electronic, dissociative, and three-body recombination. Massey and Burhop[44] discuss the different processes in some detail, so they will not be recounted here. Each one of the processes may have associated with it a coefficient of recombination which depends on pressure and temperature in a particular way. The microwave method, measuring the electron density as a function of time, leads to a recombination coefficient which is related to more than one recombination process. In many physical situations, however, the recombination coefficient for one process predominates and may be recognizable from its pressure and/or temperature dependence.

Assume that the plasma exhibits the property of quasi-neutrality ($n_+ = n_e = n$). Then, because of recombination,

$$\frac{dn}{dt} = \frac{dn_+}{dt} = \frac{dn_e}{dt} = -\alpha n_+ n_e = -\alpha n^2 \qquad (35)$$

The quantity α is the recombination coefficient. The solution of equation 35 is

$$\frac{1}{n(t)} = \frac{1}{n(o)} + \alpha t \qquad (36)$$

In the absence of other loss mechanisms, the recombination coefficient may be obtained from the slope of a linear plot of $1/n$ as a function of time.

The relative loss rate $(1/n)dn/dt$ is proportional to the electron density. Volume recombination (remote from the walls of the container) would make the density uniform, since the relative loss rate is greater in regions of higher concentrations.

As mentioned in part B 2 a, electrons and ions recombine readily at the wall of the containing vessel, so that the concentration at the wall may be assumed zero. Therefore, there is always a loss by

diffusion to the walls, but situations exist where this loss may be negligible when compared to volume recombination. Since the rate of electron loss by volume recombination is proportional to n^2, recombination would predominate with a high degree of ionization or at high pressures where the diffusion loss is reduced.

Gray and Kerr[32] have done extensive work examining the reliability of results for the recombination coefficient based on 1/n vs. time plots. They have made computations which include the loss by diffusion, and have concluded that a linear plot of 1/n vs. t does not necessarily imply a loss by recombination, unless the range of electron densities covers at least an order of magnitude. Some of the earlier recombination coefficients reported by investigators who used the microwave method may be suspect on the basis of Gray and Kerr's work, since linear plots of 1/n vs. t were employed in which the electron density ranged over a factor of only two or three. In fact, Kerr, employing the equation describing loss by diffusion alone, has pointed out that plots of 1/n vs. t may appear to be linear over small ranges of electron density. Extreme caution is advised when such plots are to be interpreted.

5. Electron Loss by Attachment

Electrons may be lost by attachment to a neutral atom or molecule whose outer electronic shell is nearly filled. The most common example is oxygen, which shows a high affinity for electrons. In the early days, investigators measured electron attachment rates by allowing electrons to drift through an attaching gas, separating electron and negative ion currents by various means and comparing the magnitudes of the electron and negative ion current[6,22,37].

When attachment is the predominant loss of electrons, the microwave method can be used to measure the attachment coefficient, ν_a. The rate of electron loss may be written as

$$\frac{dn}{dt} = -\nu_a n \qquad (37)$$

where n is the electron density.

The solution of equation 37 is simply

$$n(t) = n(o)\, e^{-\nu_a t} \tag{38}$$

The attachment coefficient can be obtained from the slope of a semi-logarithmic plot of electron density as a function of time; the slope should increase linearly with pressure at constant temperature, since the rate of attachment is proportional to the number of neutral particles present.

The relative loss rate, $(1/n)\, dn/dt$, is equal to a constant so that the spatial distribution of electrons is unaffected by the attachment process.

6. Electron Loss by a Combination of Mechanisms

The electron loss processes in a plasma do not occur singly, in general, but processes occur simultaneously. As we shall see shortly, this leads to non-linear differential equations and it is difficult to obtain the individual loss coefficients. In some physical situations, one process may predominate so that linear approximations may be made. In these situations the individual loss coefficients may be obtained.

Two examples will be discussed. The first case is in a gas in which attachment does not occur. The remaining two loss mechanisms, volume recombination and ambipolar diffusion, occur simultaneously. In the second case, that of attaching gases, the equations are written for simultaneous loss by volume recombination, ambipolar diffusion and attachment. Procedures are indicated which allow solution under specified physical conditions.

a. Loss by recombination and ambipolar diffusion. Assume that one type of positive ion and electrons are present in the afterglow, and that the positive ion density is equal to the electron density. The equation for the rate of electron density loss is

$$\frac{\partial n}{\partial t} = D_a \nabla^2 n - \alpha n^2 \tag{39}$$

where n is the electron or positive ion density, D_a is the ambipolar diffusion coefficient given in section 2 a, and α is the recombination coefficient. The boundary condition is that n is zero at the walls of the container, because of wall recombination. The equation is non-linear, separation of variables technique fails, and no exact solution is known.

The key to the method of attack in this problem is the recombination term αn^2. Since the loss by recombination is proportional to the square of the electron density, this term diminishes rapidly so that in the late afterglow the principal loss is by diffusion. One would expect, then, that the spatial distribution would approach that of the fundamental diffusion mode as described in part II 3. For example, in the case of rectangular vessels as indicated in Figure 1, the spatial distribution will become sinusoidal, as shown by equation 31. Once the spatial distribution is known, equation 39 is reducible to an equation in one variable, time.

The effect of the recombination term and higher order diffusion modes can be shown more rigorously by a machine solution of the finite difference form of equation 39. Oskam[47] has done this assuming diffusion in one dimension, using a uniform spatial distribution as the initial condition. His results indicate, as expected, that the loss by higher order diffusion modes is negligible after a sufficient time has elapsed in the afterglow. After this critical time, the loss can be described essentially by recombination and the fundamental diffusion mode whose spatial density distribution is known. This critical time occurs when the density is a factor of four or five above the value obtained from the straight line representing the decay of the fundamental diffusion mode alone.

If the sinusoidal spatial density distribution of the fundamental diffusion mode is assumed, then equation 39 reduces to*

$$\frac{dn_o(t)}{dt} = -kn_o(t) - \alpha n_o^2(t) \qquad (40)$$

where n_o is the electron density at the center of the rectangular

* See Appendix

vessel whose dimensions are a x b x c, and the constant is given by

$$k = D_a \pi^2 \left(\frac{1}{a^2} + \frac{1}{b^2} + \frac{1}{c^2} \right) \tag{41}$$

The solution of equation 40 is

$$n_o(t) = \frac{C_1 k e^{-kt}}{1 - \alpha C_1 e^{-kt}} \qquad \text{where } C_1 = \frac{n_o(o)}{k + \alpha n_o(o)} \tag{42}$$

Obtaining the ambipolar diffusion coefficient and recombination coefficient from a plot of $n_o(t)$ as a function of time and equation 42 is somewhat of a problem in itself.

Some authors[14,50] write equation 42 in the form

$$\frac{n_o(t)}{1 + \frac{\alpha n_o(t)}{k}} = \frac{n_o(o)}{1 + \frac{\alpha n_o(o)}{k}} e^{-kt} \tag{43}$$

and adjust the factors α, k, and $n_o(o)$ for a best fit to the data points (comparing both sides of equation 43). In the present work a different approach is used. Equation 40 is written in the finite difference form

$$\frac{1}{n_o(t)} \quad \frac{\Delta n_o(t)}{\Delta t} = - k - \alpha n_o(t) \tag{44}$$

and the left hand side of the equation is plotted as a function of $n_o(t)$. The coefficients k and α are found from the intercept and slope of the resulting straight line, using the method of least square deviation. In order to achieve accuracy with this method, $n_o(t)$ must be found at small increments of time, which requires a large amount of data and routine calculation. Since the routine calculation could be done by machine (IBM 650 Digital Computer was used), it was felt that this method was superior to the method employing equation 43. The present method leads directly to D_a and α, while the previous method required adjustment of parameters for a best fit to data points.

b. Loss by recombination, ambipolar diffusion, and attachment. The equations describing the charged particles of the plasma in the afterglow of an electronegative gas are:

$$\frac{\partial n_e}{\partial t} = D_{ae} \nabla^2 n_e - \nu_a n_e - \alpha_e n_e n_+$$

$$\frac{\partial n_-}{\partial t} = D_{a-} \nabla^2 n_- + \nu_a n_e - \alpha_- n_+ n_- \qquad (45)$$

$$\frac{\partial n_+}{\partial t} = D_{a+} \nabla^2 n_+ - \alpha_- n_+ n_- - \alpha_e n_+ n_e$$

The electron density, positive ion density, and negative ion density are n_e, n_+, and n_- respectively. The first term on the right hand side of each equation represents the loss by ambipolar diffusion and the ambipolar diffusion coefficients are given by equations 25. ν_a is the attachment coefficient, α_- is the negative ion-positive ion recombination coefficient, and α_e is the electron-positive ion recombination coefficient. The first equation relates the rate of change of electron density to losses by ambipolar diffusion, attachment to neutral particles, and recombination with positive ions. The second equation relates the rate of change of the negative ion density to losses by ambipolar diffusion and recombination with positive ions. This equation has a source term $\nu_a n_e$ which describes the formation of negative ions by attachment. The last equation relates the rate of change of the positive ion density to losses by ambipolar diffusion, and recombination with both electrons and negative ions.

Since the microwave method of measurement is responsive only to the electron constituent of a plasma, only the electron density as a function of time may be obtained. The possibility of obtaining electron loss coefficients from equations 45 by the microwave method therefore appears remote, expecially when it is noticed that the equations are not only coupled through the various constituent densities, but also through the ambipolar diffusion coefficients (in equations 25, the factor "a" is the ratio of n_- to n_e). There are some simplifications which may be made in certain physical situations, however.

The easiest interpretation of data occurs when the diffusion terms in equations 45 are negligible. Such a situation occurs at higher pressures, where the diffusion loss is hampered by the increased elastic collision process with neutral particles. If, in addition, the negative-ion constituent of the plasma is negligible, the requirement of charge neutrality requires that $n_e = n_+$ and the equation describing the electrons in 45 becomes uncoupled from the remaining two.

$$\frac{\partial n_e}{\partial t} = - \nu_a n_e - \alpha_e n_e^2 \qquad (46)$$

This equation may be used to obtain the attachment coefficient and recombination coefficient by a method similar to the one described in the previous section.

The negative ion density may become negligible for two different reasons. First, the cross-section for recombination of the negative ions and positive ions is much larger than the cross-section for the recombination of the electrons and positive ions. The negative ions will therefore disappear much faster than the electrons. Secondly, the production of the negative ions may be reduced by using low partial pressures of the electronegative gas and using a "buffer gas" to increase the total pressure to a value where loss by diffusion is negligible. Kasner, Rogers and Biondi[34] have used this method in the study of recombination in oxygen. Neon was used for a buffer gas. The ionization potential of neon is sufficiently high so that one observes only ions of oxygen. Electron attachment should not be a significant factor since the oxygen partial pressure was low compared to the total pressure. In this last case, equation 46 would be reduced to loss by recombination only as discussed in part II B 4.

In the presence of ambipolar diffusion the situation appears to be extremely difficult. Equations 45 then are nonlinear and no general solutions are known. The densities are functions of both space and time and the spatial distributions are difficult to ascertain. At low electron densities, with a low degree of ionization,

the electron-positive ion recombination loss will be small, and the spatial distribution will approach that of the lowest diffusion mode (described in part II B 3). Even though the spatial distribution is known, and recombination is negligible, equations 45 are still coupled and additional assumptions on the presence of the negative ion are required before the equations are soluble. If the negative ions formed disappear very rapidly, D_{ae} becomes independent of the densities, so that the first of the equations 45 is decoupled from the other two and is soluble.

The problem in the general solution of equations 45 is quite insurmountable, and, as pointed out in the previous discussion, only in a few special cases may the loss process coefficients be obtained by microwave methods in electronegative gases. In these special cases, a large amount of ingenuity is required on the part of the experimenter in setting up physical conditions so that the loss process coefficients may be interpreted from the data.

C. Relation of Microwave Measurements to Plasma Parameters

The complex conductivity of a weakly ionized plasma at microwave frequencies has been found in part II A. If the complex conductivity is obtained experimentally, then the electron density and collision frequency for momentum transfer may be found by equations 9 and 10. It is now necessary to relate the measurable quantities of phase shift and attenuation of the microwave signal to the complex conductivity. Two cases are of interest. If recombination is predominant in an afterglow, the spatial distribution of the electrons would be expected to be uniform (see section on recombination, II B 4). In this case, the relation of phase shift and attenuation of a microwave signal passing through the plasma to the electron density and collision frequency is easily derived.

If diffusion is the predominant loss mechanism, the electron gas is not uniformly distributed and the relationship of the measurable quantities and the plasma parameters is not straightforward. In this second case, an excellent approximation method has been developed by Anderson and Goldstein[2]. This method is briefly outlined, and the simplifying assumptions required for solution are identified.

1. Uniform Electron Density Distribution

The wave equation for the electric field intensity, $\bar{E}$, of an electromagnetic wave passing through a homogeneous lossy medium is well known and is given by

$$\nabla^2 \bar{E} = j\omega\mu \left(\sigma + j\omega\epsilon \right) \bar{E} \tag{47}$$

It has been assumed here that the time variation of $\bar{E}$ is sinusoidal and that the time variation is written in the form $e^{j\omega t}$. ω is the radian frequency and the medium is described by μ, ϵ, and σ which are the permeability, permittivity, and conductivity respectively. The permeability and permittivity of free space will be used, and the plasma will be described by a complex conductivity as discussed in part II A.

The solutions of the wave equation may be divided into the familiar transverse electric and transverse magnetic modes in a waveguide. The following discussion assumes the dominant TE_{10} mode, since the experiments were carried out in a rectangular waveguide at a frequency where all other modes were cut off. A parallel discussion may be used for a cylindrical waveguide. If the geometry is assumed to be that of Figure 1, with field variations in the z direction of the form $e^{-\gamma z}$, the complex propagation constant, γ, may be found by solving the wave equation with the boundary conditions of Figure 1. For the TE_{10} mode, γ is

$$\gamma = \sqrt{\left(\frac{\pi}{a}\right)^2 - \omega^2 \mu_o \epsilon_o + j\omega\mu_o\sigma} = \alpha + j\beta \tag{48}$$

The real part of the propagation constant, α, is the attenuation/length, and the imaginary part, β, is the phase shift/length. For a uniform plasma filling the cell, the conductivity is given by equation 8, which is rewritten in the form

$$\sigma = \frac{nq^2}{m} \left[\frac{\nu_m - j\omega}{\nu_m^2 + \omega^2} \right] \tag{49}$$

It is noted from equations 48 and 49 that if the complex propagation constant is measured, then the electron density, n, and collision frequency, ν_m, are obtainable.

If ℓ is the length of the plasma filled waveguide cell, an electromagnetic wave is attenuated by a factor $e^{-\alpha\ell}$ in passing through the plasma. $\beta\ell$ is the phase change of the wave as it passes through the cell. The phase shift actually measured is the change in phase that takes place when the cell is changed from the un-ionized condition to an ionized condition. This may be written as

$$\phi = \beta_o \ell \quad -\beta\ell \tag{50}$$

where ϕ is the measured change in phase, β_o is the phase shift constant when there is no plasma in the cell ($\sigma = 0$) and β is the phase shift constant when the gas is ionized (given by equation 48). The method of experimentally determining ϕ and $\alpha\ell$ will be described in part III in the description of the microwave bridge circuit.

Equation 48 may be separated into real and imaginary parts, so that explicit equations may be found for the electron density and collision frequency in terms of the phase shift and attenuation. The results are given conveniently in equation 51 in terms of dimensionless variables which are then defined.

$$X = \frac{4A^2 \left(\sqrt{1 - S^2} - B \right)^2}{A^2 + 2\sqrt{1 - S^2} B - B^2} + A^2 + 2\sqrt{1 - S^2} B - B^2$$

$$Z = \frac{2A \left(\sqrt{1 - S^2} - B \right)}{A^2 + 2\sqrt{1 - S^2} B - B^2} \tag{51}$$

where

$$X = \left(\frac{\omega_p}{\omega}\right)^2 \qquad Z = \frac{\nu_m}{\omega}$$

$$\omega_p^2 = \frac{nq^2}{\epsilon_o m} \qquad S = \frac{\omega_c}{\omega}$$

$$A = \frac{\alpha c}{\omega} \qquad B = \frac{\phi c}{\ell \omega}$$

ω_p is the plasma frequency, ω is the operating radian frequency, c is the velocity of light $(\mu_o \epsilon_o)^{-1/2}$, and ω_c is the cut-off radian frequency for the TE_{10} mode for the empty waveguide (equal to $\pi c/a$).

2. An Approximate Method for Non-Uniform Electron Density Distributions

It was determined in part II B 4 that in an afterglow controlled by recombination, the electron density approaches a uniform spatial distribution. In such a situation the attenuation and phase constants of an electromagnetic wave passing through the plasma may be calculated exactly by the method described in the previous section. When the plasma is non-uniform, it is difficult to relate the measurable phase shift and attenuation to the electron density and collision frequency of a plasma. In a waveguide containing a homogeneous medium, the solution of the wave equation separates into modes which are independent of each other. In the inhomogeneous case, it is very difficult to obtain an exact solution that may be used in practical measurements. An excellent discussion of an exact method of solution for waves on inhomogeneous cylindrical structures has been given by Adler[1].

The method used here is an approximate one, but one which readily adapts itself to the calculation of electron density and collision frequency of a plasma from experimentally determined phase shift and attenuation measurements. The basic assumption is that the fundamental mode propagated in the empty waveguide is perturbed only by a small amount when a weakly ionized plasma fills the waveguide. This assumption is valid at high frequencies, where the conductivity, σ, in equation 48 is small. This method is not applicable in situations where the plasma frequency approaches the value of the operating frequency, where the conductivity term becomes appreciable.

Maxwell's equations for the plasma medium may be written in terms of the complex conductivity as

$$\nabla \times \bar{E} = - j \omega \mu_o \bar{H}$$

$$\nabla \times \bar{H} = (\sigma_r + j \sigma_i + j \omega \epsilon_o) \bar{E} \qquad (52)$$

If $\bar{E}$ and $\bar{H}$ are expressed as complex values, the time averaged complex power flow through a closed surface is given by

$$\text{Power} = \int_A 1/2\ (\bar{E} \times \bar{H}^*) \cdot d\bar{a} \tag{53}$$

where the asterisk denotes the complex conjugate. By use of the divergence theorem and Maxwell's equations, this may be manipulated into the form

$$\int_A (\bar{E} \times \bar{H}^*) \cdot d\bar{a} = - \int_V \sigma_r \bar{E}\cdot\bar{E}^* dv + j\omega \int_V (\epsilon_o + \frac{\sigma_i}{\omega})\ \bar{E}\cdot\bar{E}^*\ dv$$

$$- j\omega\mu_o \int_V \bar{H}\cdot\bar{H}^*\ dv \tag{54}$$

Only the ends of the plasma filled waveguide section contribute to the integral on the left hand side of equation 54, since the walls are assumed perfeatly conducting. The field intensities may be expressed as the vector sum of two quantities; the first a component in the direction of propagation (H_z and E_z), and the second a vector transverse to the direction of propagation ($\bar{H}_t$ and $\bar{E}_t$). For TE modes the field intensities are related by the expressions

$$1_z \times \bar{E}_t = \frac{j\omega\mu_o}{\gamma}\ \bar{H}_t$$

and

$$\bar{H}_t = \frac{-\gamma}{\gamma^2 + \omega^2\mu_o\epsilon_o}\ \nabla_t H_z$$

where $\nabla_t H_z$ is the gradient in the transverse plane. Thus all field quantities may be expressed in terms of the transverse electric field intensity, E_t. If we assume field variations in the z direction along the waveguide axis of the form $e^{-\gamma z}$ where $\gamma = \alpha + j\beta$, then we may divide equation 54 into real and imaginary parts with the result:

$$\frac{\frac{1}{\omega\epsilon_o}\iint \sigma_r |E_t|^2 da}{\iint |E_t|^2 da} = \frac{2\alpha\beta}{\omega^2\mu_o\epsilon_o}$$

$$\frac{-\frac{1}{\omega\epsilon_o}\iint \sigma_i |E_t|^2 da}{\iint |E_t|^2 da} = \frac{1}{\beta_{of}^2}(\alpha^2 - \beta^2 + \beta_o^2) \qquad (55)$$

where

β_{of} = phase shift constant (radians/meter) of a free space (unguided) wave; it is equal to ω/c.

β = phase shift constant of the guided wave in a plasma-filled waveguide.

β_o = phase shift constant of the guided wave in an empty waveguide.

The integrations are to be carried out over the cross-section of the waveguide. If the electrons are distributed uniformly, the conductivity terms can be taken outside the integral signs and the integrals would cancel. This leads to the result given in the previous section. Equations 55 may be used to integrate the non-uniformities of the conductivity over the cross-section of the waveguide and it is noticed that, in effect, the conductivity is weighted and averaged by the square of the electric field intensity.

If ℓ is the length of the plasma-filled section, equations 55 may be written in terms of the total attenuation $\alpha\ell$ and the phase shift ϕ which are measurable quantities. ϕ again is the change in phase shift that takes place when the cell is changed from the un-ionized condition to the ionized condition and is given by equation 50.

$$\frac{\frac{1}{\omega\epsilon_o}\iint \sigma_r |E_t|^2 da}{\iint |E_t|^2 da} = \frac{2(\alpha\ell)\left[\sqrt{\frac{\omega^2}{c^2} - \frac{\pi^2}{a^2}}\,\ell - \phi\right]}{\ell^2\,\omega^2/c^2} \qquad (56)$$

$$-\frac{1}{\omega\epsilon_o}\frac{\iint \sigma_i |E_t|^2 \, da}{\iint |E_t|^2 \, da} = \frac{c^2}{\omega^2}\left[\frac{(\alpha\ell)^2}{\ell^2} + \frac{2\sqrt{\frac{\omega^2}{c^2} - \frac{\pi^2}{a^2}}\,\phi}{\ell} - \frac{\phi^2}{\ell^2}\right] \tag{56}$$

The special example of interest here is to relate the electron density and collision frequency to the measurable attenuation and phase shift when diffusion is the predominant loss mechanism. It was shown in part II B 3 that in the rectangular waveguide cell, diffusion leads to a sinusoidal spatial distribution of electrons. The collision frequency for momentum transfer, ν_m, will be assumed to be spatially independent. This should be approximately correct, since ν_m is a function of the electron energy, and it is assumed that thermal gradients are absent in the late afterglow. Under these assumptions, σ_r and σ_i both have sinusoidal variations in both the x and y directions. E_t for a TE_{10} mode has only a y direction component and the amplitude varies sinusoidally in x. Using these variations and letting n_o be the electron density along the centerline of the waveguide cell, equations 56 become

$$\frac{1}{\omega\epsilon_o}\frac{\iint \sigma_r |E_t|^2 da}{\iint |E_t|^2 \, da} = \frac{16\, n_o q^2}{3\pi^2 \omega\epsilon_o}\left(\frac{\nu_m}{\nu_m^2 + \omega^2}\right)$$

$$-\frac{1}{\omega\epsilon_o}\frac{\iint \sigma_i |E_t|^2 \, da}{\iint |E_t|^2 \, da} = \frac{16\, n_o q^2}{3\pi^2 \omega\epsilon_o}\left(\frac{\omega}{\nu_m^2 + \omega^2}\right) \tag{57}$$

Finally, equations 55 and 57 may be solved for the electron density and collision frequency. The results, written in dimensionless form, are

$$X = \frac{3\pi^2}{16}\left[\frac{4A^2\left(\sqrt{1 - S^2} - B\right)^2}{A^2 + 2\sqrt{1 - S^2}\,B - B^2} + A^2 + 2\sqrt{1 - S^2}\,B - B^2\right]$$

$$Z = \frac{2A\left(\sqrt{1 - S^2} - B\right)}{A^2 + 2\sqrt{1 - S^2}\,B - B^2} \tag{58}$$

where the parameters are those defined in equations 51. The same phase shift and attenuation measurement would lead to an electron density at the center of the waveguide for the sinusoidal distribution $3\pi^2/16$ (approximately 1.85) times the value obtained in a uniform distribution.

Equations 51 are used to obtain the plasma parameters in the early afterglow when the electron density is high and recombination is the principal loss mechanism. Equations 58 are used in the late afterglow when the plasma is controlled by diffusion and the spatial distribution is sinusoidal.

D. Measurements of the Radiation Temperature

The problem of electron temperature measurements during the plasma afterglow has to date received little attention. Originally investigators estimated the time required for electron energy to relax to thermal equilibrium with the heavier gas constituents following the removal of the excitation source. They assumed that the time required to achieve thermal equilibrium is dependent primarily on the electron energy decrease through elastic collisions of the electrons with neutral particles. Results of different microwave measurements in nitrogen afterglows have been in disagreement. Formato and Gilardini[29] have pointed out the possibility of the presence of energetic electrons coming from ionizing collisions of long-lived metastable molecules, providing for an increase in electron energy. Thus time estimates for reaching thermal equilibrium based on elastic collisions may be too short, and some results of microwave measurements reported as carried out with room temperature electrons may have actually involved more energetic electrons. Thus the need for electron temperature monitoring is established as one of the fundamental requirements for a complete interpretation of afterglow experiments.

The basic problem of relating the electron temperature to the power radiated at microwave frequencies is in accounting for the absorption. In a model of a radiating hot body, Kirchhoff's radiation law relates the temperature of the body to the ratio of emission to

absorption of the body. Bekefi[10,11] has used this classical model to describe a method of measuring electron temperatures without knowledge of the absorption of a plasma. Kirchhoff's law may be written as

$$P_\omega = B\ (\omega,T)\ A_\omega$$

where $P_\omega d\omega$ is the radiation intensity in the frequency range ω to $\omega + d\omega$, $B\ (\omega,T)$ is the intensity of black-body radiation, and A_ω is the absorptivity of the plasma. A_ω varies from unity for a black body to zero for a non-absorbing body.

In order to determine the temperature of a body by direct measurement of the radiation intensity, P_ω, the absorptivity, A_ω, would have to be obtained separately. The technique used in this thesis is to compare the radiation from the plasma with a known variable standard radiating through the plasma to the observer, as shown in Figure 3.

Let the plasma temperature be denoted by T_p and the temperature of a known variable black-body source as T_s. The emission from the known source is $B\ (\omega,T_s)$. If this radiation passes through the plasma, a fraction A_ω is absorbed. Referring to Figure 3, an observer on the opposite side of the plasma would therefore receive a fraction $1 - A_\omega$ of the standard source's radiation intensity. Adding the intensity of the plasma radiation, the total intensity seen by an observer on the opposite side of the plasma from the variable standard would be

$$P_{01} = (1 - A_\omega)\ B\ (\omega,T_s) + A_\omega B\ (\omega,T_p) \qquad (60)$$

The reflectivity is assumed to be zero. If the plasma were removed from the path between the observer and the known source, the total intensity received would be simply

$$P_{02} = B\ (\omega,T_s) \qquad (61)$$

The difference in intensities in the two cases is

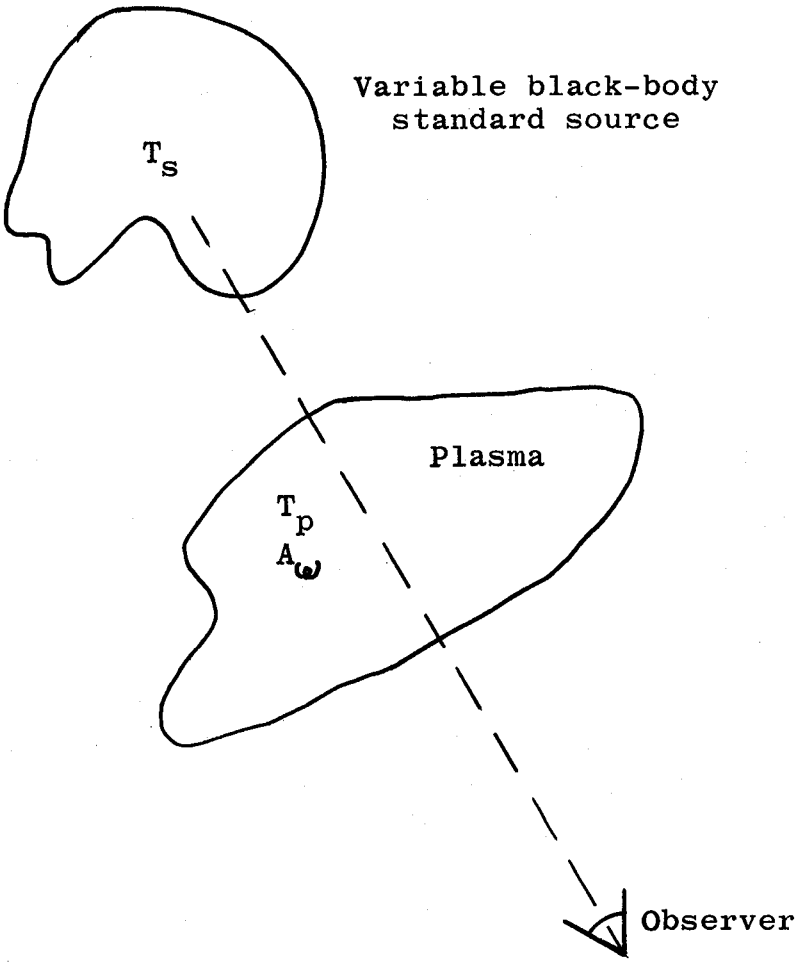

Fig. 3. Arrangement for radiation measurements.

$$\Delta P_0 = P_{01} - P_{02} = A_\omega \left[B(\omega, T_p) - B(\omega, T_s) \right] \qquad (62)$$

When ΔP_0 is zero, $T_p = T_s$, regardless of the value of the absorption term A_ω.

The measurement of the plasma temperature is obtained by periodically inserting the plasma between the observer and the standard, adjusting the standard until $\Delta P_0 = 0$. When this null is obtained, the plasma temperature is equal to the known standard temperature. The details of the experimental arrangement for temperature measurements and a description of the radiometer are included in part III D.

Since the emission at microwave frequencies in weakly ionized plasmas is mainly the result of the motion of free electrons (bremsstrahlung emission from collisions of electrons and neutrals), the temperature measured will be that of the electron gas. However, in assigning an electron temperature, the velocity distribution is assumed Maxwellian. If the velocity distribution function is other than Maxwellian, the parameter measured is a fictitious temperature, still related to the mean electron energy, but through the velocity distribution function, which may not be known[12]. A Maxwellian distribution is expected in the afterglow unless a source mechanism, such as the release of metastable energy, is present.

E. Relation of Cross-Section to Collision Frequency

Collision frequency in a gas is defined as the mean velocity of a particle divided by the mean distance traveled between collisions. In a general sense, the word collision may describe any interaction such as recombination, excitation, "billiard ball" type elastic collision, etc. In a weakly ionized gas the dominant collision process involves the elastic scatter of electrons by neutral particles. It is advantageous to introduce a cross-section for momentum transfer to describe such a process.

The total scatter cross-section is defined as:[40]

$$Q_o(v) = \int_0^\pi 2\pi I_o(\theta) \sin\theta \, d\theta \qquad (63)$$

where $I_o(\theta)$ is the angular distribution function for scatter into the angle between θ and $\theta + d\theta$, where θ is measured in center of mass coordinates.

For an elastic collision between an electron and a neutral molecule, the speed of the electron is essentially unchanged[41]. The change in momentum of the electron along its initial direction is thus

$$\text{Change in momentum} = \mu v (1 - \cos\theta) \tag{64}$$

where μ is the reduced mass

$$\mu = \frac{mM}{m + M} \tag{65}$$

and the neutral particle is considered to be stationary.

The mean fractional change in momentum is therefore related to the mean value of $(1 - \cos\theta)$, which is

$$\langle 1 - \cos\theta \rangle = \frac{\int_o^\pi 2\pi(1 - \cos\theta) I_o(\theta) \sin\theta \, d\theta}{\int_o^\pi 2\pi I_o(\theta) \sin\theta \, d\theta} = \frac{Q_m}{Q_o} \tag{66}$$

where Q_m is

$$Q_m = \int_o^\pi 2\pi (1 - \cos\theta) I_o(\theta) \sin\theta \, d\theta \tag{67}$$

and Q_m is referred to as the cross-section for momentum transfer.

If the model of the collision is taken as that of hard spheres, the mean value of $(1 - \cos\theta)$ is unity, so that Q_m and Q_o are equal. This corresponds to an angular distribution function $I_o(\theta)$ independent of θ. For very slow electrons this is a good approximation[42]. In this case the collision frequency for momentum transfer may be defined as

$$\nu_m = N Q_m v = N Q_o v \tag{68}$$

since the mean free path is equal to the reciprocal of the molecular number density times the cross-section. v is the mean velocity and for a Maxwellian distribution is $(8kT / \pi m)^{1/2}$.

The molecular number density is usually given in terms of the pressure normalized to $0^{\circ}C$ or

$$N = 3.54 \times 10^{16} p_o \text{ (particles/cm}^3\text{)} \tag{69}$$

where p_o is in mm of mercury and is equal to

$$p_o = p \frac{273}{T} \tag{70}$$

Thus using equations 68, 69 and 70, the cross-section for momentum transfer may be found from the collision frequency.

PART III.

APPARATUS AND METHOD OF PROCEDURE

A. The Plasma Cell

In previous microwave transmission method experiments, a standard X-band waveguide has been tapered into a square section and a cylindrical glass tube with tapered ends has been placed in this square section to form the plasma cell.[13,29] The discharge takes place between electrodes placed external to the waveguide on each end of the glass cell. The positive column of a glow discharge is formed in the cylindrical glass tube within the waveguide.

In the present experiment, the cell consists of a length of OFHC X-band waveguide with bakeable windows on each end. The entire cell is constructed of ultra-high vacuum materials suitable for bakeout to 400° centigrade. Holes are drilled in the top of the waveguide and anode wires extend down to these holes flush with the top of the waveguide. The waveguide acts as a hollow cathode and the negative glow of the discharge spreads down into the cell and out to several inches from the anode. The cell has two anodes approximately seven inches apart in order to provide a longer interaction path for the microwave signal.

The advantages of the cell are twofold. First, the questionable approximations and assumptions necessary with the enclosed glass cylinder mentioned previously are removed. The tapered glass cylinder causes some question as to the effective length of the microwave-plasma interaction and accounting for the presence of the glass involves approximations in obtaining the wavelength of the microwave signal in the cell. The rectangular cross-section of the waveguide cell provides a simple shape for calculation of the microwave-plasma interaction. The second advantage is the fact that the electron temperature in the hollow cathode negative glow does not rise as high as the electron temperature in a positive column. The electron temperature would then be expected to drop to room temperature faster in the negative glow, giving a longer period for obtaining data in an isothermal plasma.

The disadvantage of the cell is that the pressure range of operation is limited by the spread of the discharge into the waveguide. In nitrogen, for example, discharges were obtained in the range 0.2 to about 7.5 millimeters of mercury. In helium, discharges were obtained from 0.5 up to approximately 30 or 40 millimeters of mercury.

The pressure range might be increased by increasing the size of the anode holes in the top of the waveguide. This has the adverse effect of increasing the reflections of the microwave signal, however. Some compromise must be made. At present, the hole size is 3/16" and the pressure range of operation is that mentioned in the previous paragraph. The voltage standing wave ratio of a single 3/16" hole in X-band waveguide is less than 1.05. The VSWR of the complete cell is approximately 1.01. In order to obtain such a low VSWR, it was necessary to take swept frequency measurements on the cell and to pick an optimum frequency of operation.

B. The Vacuum System

A block diagram of the vacuum system is shown in Figure 4. All parts included in the "oven limits" are constructed of suitable ultra-high vacuum materials and are bakeable to at least 400° centigrade. This section of the vacuum system is isolated from the remainder of the system by activated alumina traps which have a high affinity for the low vapor pressure organic oils used in the diffusion pump and manometer.[27]

Measurements of pressure were obtained during roughing with a Veeco Type DVM1 thermocouple gauge. The system was baked at approximately 400° centigrade for approximately twenty-four hours while pumping with an oil diffusion pump (Consolidated Electrodynamic Corp. Type MCF-61) to drive absorbed and adsorbed gases from the walls of the system. Following the baking, the metal ultra-high vacuum valves, numbered 1 and 4 in Figure 3, were closed, and the closed system was pumped to ultra-high vacuum pressures by an Ultek Series 150 vac-ion pump. The pressures were measured by a Veeco RG75 ion

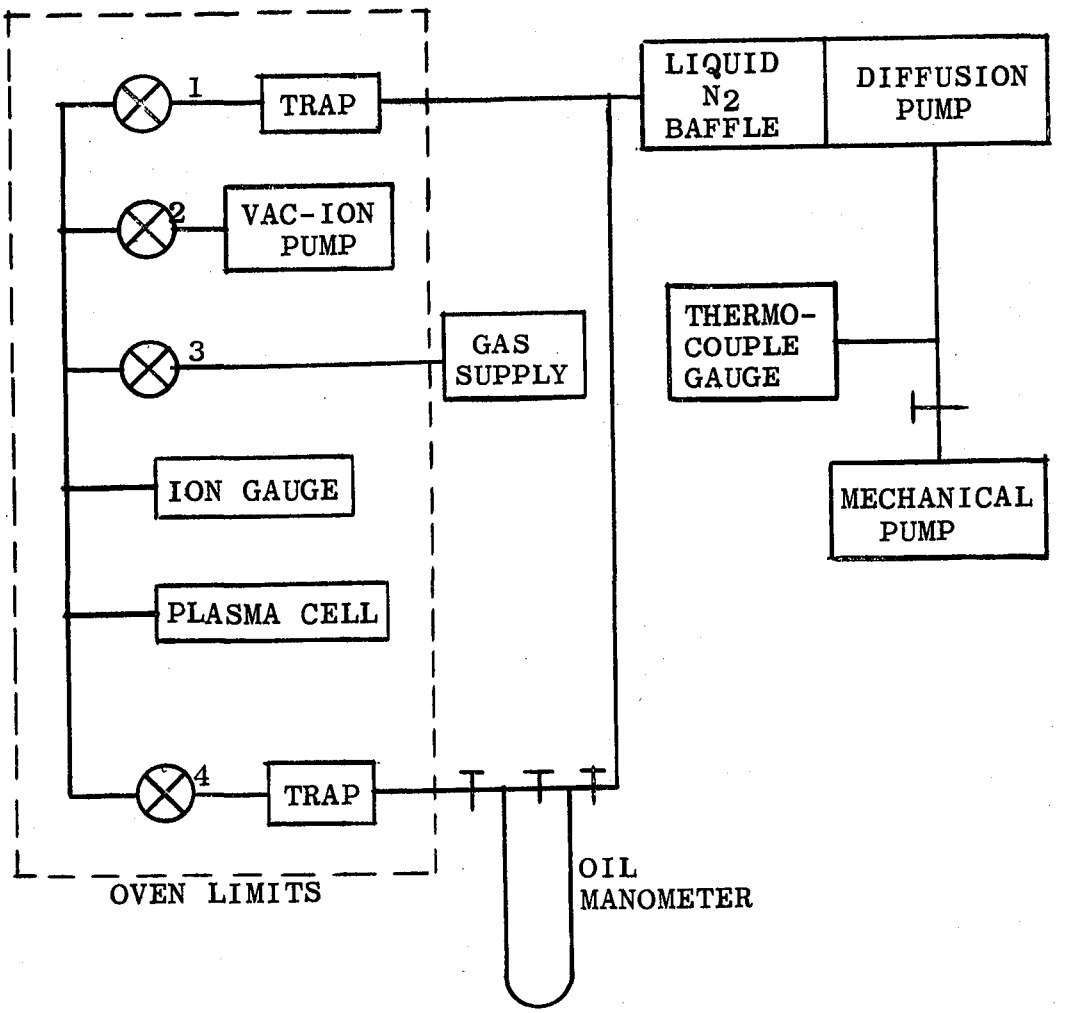

Granville Phillips Type C Ultra-high vacuum valves

High vacuum ground glass stopcock

Fig. 4. Vacuum system.

gauge which had a low range of 10^{-9} mm of mercury, and since this range was achieved, the ultimate vacuum reached is not known, but is at least 10^{-9} mm of mercury. The clean vacuum system leak rate is less than 10^{-10} mm of mercury/minute. Since experiments were carried out at pressure in the vicinity of 1 mm of mercury, the impurity level due to vacuum system material contamination was less than 1 part in 10^{8}. Gas samples used in all experiments were Linde Co. MSC (mass-spectrometer controlled) grade samples. These have a maximum impurity level of 10 parts per million for rare gases and 100 parts per million for diatomic gases. These samples were leaked into the test cell through an ultra-high vacuum valve. Pressures in the experimental range were measured with a low vapor pressure oil (Octoil-S) manometer isolated from the test section by an activated alumina trap.

C. The Microwave Bridge Circuit

The microwave circuit used to obtain measurements of the phase shift and attenuation of a microwave signal passing through a decaying plasma is an extension of a basic microwave interferometer. In an interferometer circuit, a portion of the signal is coupled into a branch bypassing the plasma vessel and is then mixed with the signal passing through the plasma by use of a three port "T" junction. It is described adequately, for example, in S. C. Brown's book on Basic Data of Plasma Physics[18]. The interferometer pattern caused by a decaying plasma goes through maxima and minima corresponding to the phase shift of the microwave signal passing through the decaying plasma. The amplitude of the fringe pattern is related to the attenuation of the same signal.

The idea for the circuit used in these experiments came from an article by R. F. Whitmer[56], who suggested that it might be possible to mix the interferometer signals in a hybrid T junction and obtain direct measurement of attenuation and phase shift from the two output arms of the hybrid T.

That this is indeed the case may be seen by considering the properties of such a junction shown in Figure 5. Assume the electric

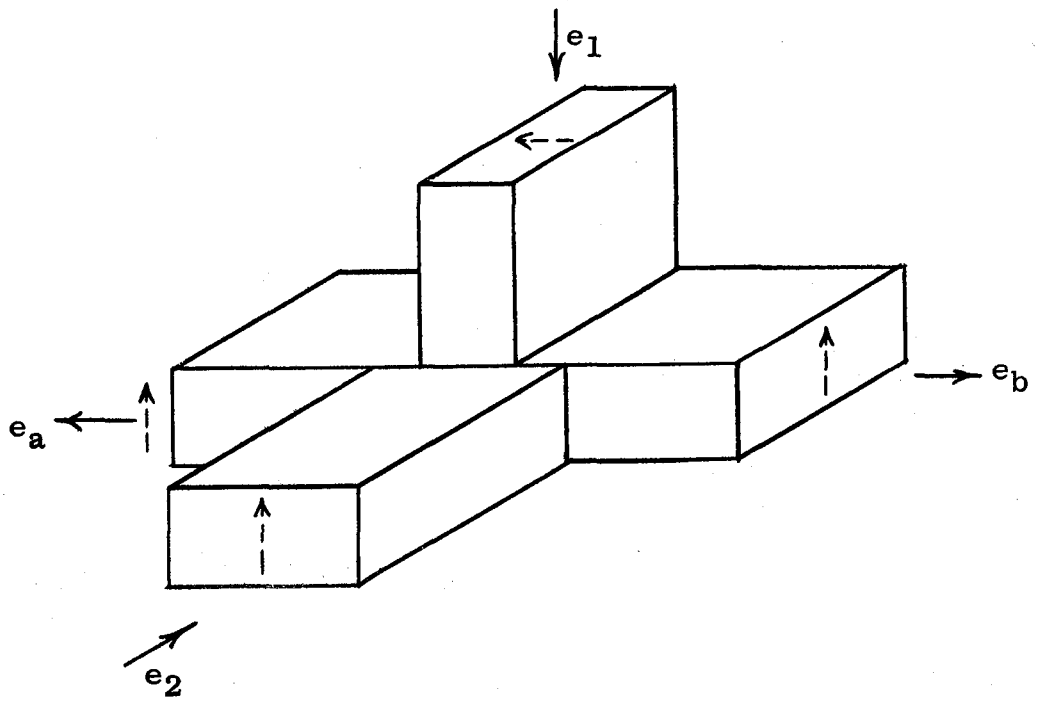

Fig. 5. Hybrid T detector.

fields of the TE_{10} mode are in the directions of the dotted arrows drawn at faces of the ports. The properties of the junction are that the electric field entering port 1 is split into equal fields leaving ports a and b with a phase reversal in port b. The signal entering port 2 is split equally into signals leaving ports a and b with no phase reversals. There is no coupling between ports 1 and 2. Thus the instantaneous values of the electric field intensities may be given by

$$e_a = \frac{e_2 + e_1}{2} \quad , \quad e_b = \frac{e_2 - e_1}{2} \tag{71}$$

If it is assumed that e_1 is the electric field intensity of a reference signal and e_2 is this same reference signal after being attenuated and phase shifted by a decaying plasma (or any other cause), the fields may be expressed mathematically as

$$e_1 = E_1 e^{j\omega t} \quad , \quad e_2 = E_1 e^{j\omega t}\ e^{-A}\ e^{-j\phi} \tag{72}$$

where A is the attenuation of the signal entering port 2 in nepers and ϕ is the shift in phase of this signal from the reference signal. If equations 72 are substituted in equations 71, the electric fields at the output arms may be obtained.

$$\begin{aligned} e_a &= \frac{1}{2} E_1 e^{j\omega t} \left[e^{-A}\ e^{-j\phi} + 1 \right] \\ e_b &= \frac{1}{2} E_1 e^{j\omega t} \left[e^{-A}\ e^{-j\phi} - 1 \right] \end{aligned} \tag{73}$$

The magnitudes of e_a and e_b are of interest, since the magnitude is the quantity detected by a crystal detector mount. If the magnitudes are expressed as E_a and E_b, it may be found that

$$E_a = \frac{E_1}{2} \left[1 + 2e^{-A} \cos\phi + e^{-2A}\right]^{1/2}$$

$$E_b = \frac{E_1}{2} \left[1 - 2e^{-A} \cos\phi + e^{-2A}\right]^{1/2} \quad (74)$$

A family of constant attenuation curves on a plot of E_b versus E_a may be obtained by eliminating ϕ from equations 74. This is easily accomplished by squaring both sides of equations 74 and adding. The result is

$$E_a^2 + E_b^2 = \frac{E_1^2}{2} \left(1 + e^{-2A}\right) \quad (75)$$

which is the equation of a circle with radius

$$R = \frac{E_1}{2} \left(1 + e^{-2A}\right)^{1/2}$$

Eliminating the attenuation, A, from equations 74 results in a family of quartics for constant phase lines given by

$$E_a^4 - 2E_a^2E_b^2 + E_b^4 = E_1^2\cos^2\phi \left(E_a^2 + E_b^2\right) - E_1^4\cos^2\phi \quad (76)$$

These results are shown graphically in Figure 6. Thus if E_a and E_b are measured, it is possible to obtain the attenuation, A, and phase shift, ϕ, from Figure 6. Note that the characteristics of the hybrid T blend well to afterglow problems where the attenuation is low.

The microwave circuit is shown schematically in Figure 7. The circuit is initially balanced ($E_b = 0$) with the precision phase shifter in the lower arm and the attenuator in the upper arm. It is then possible to calibrate the bridge by employing the precision phase shifter and precision attenuator to plot a characteristic similar to Figure 6. In practice, the Figure 6 characteristic will be distorted somewhat by the nonlinear characteristics of the crystals and the non-ideal properties of the hybrid T detector. An actual calibration is shown in Figure 8.

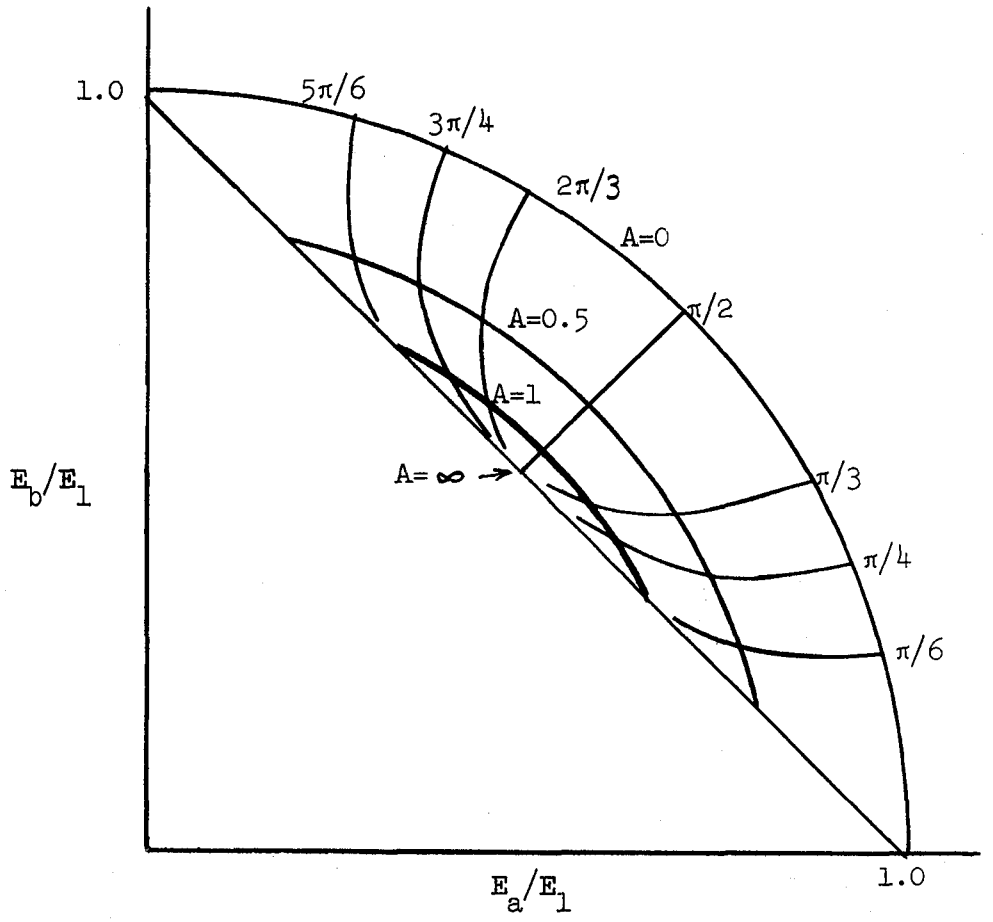

Fig. 6. Hybrid T characteristics.

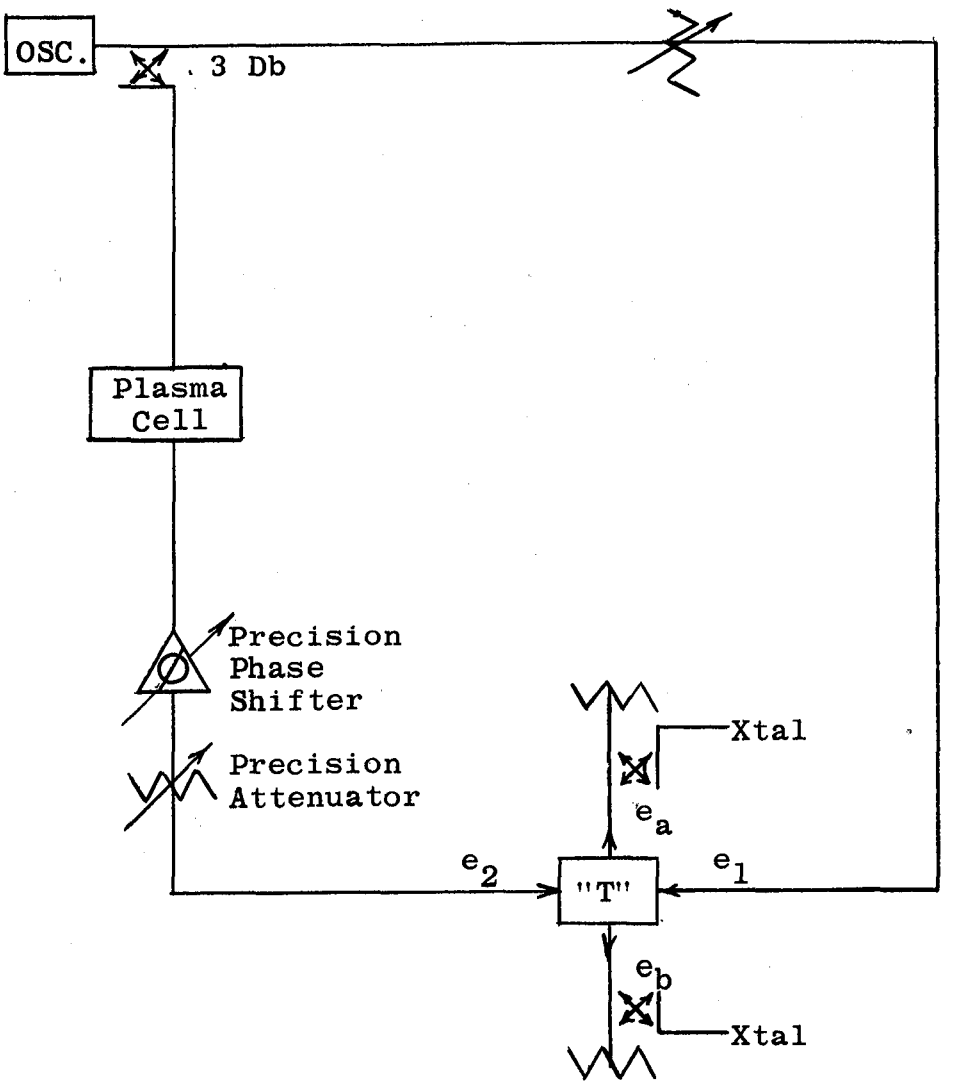

Fig. 7. Basic microwave bridge circuit.

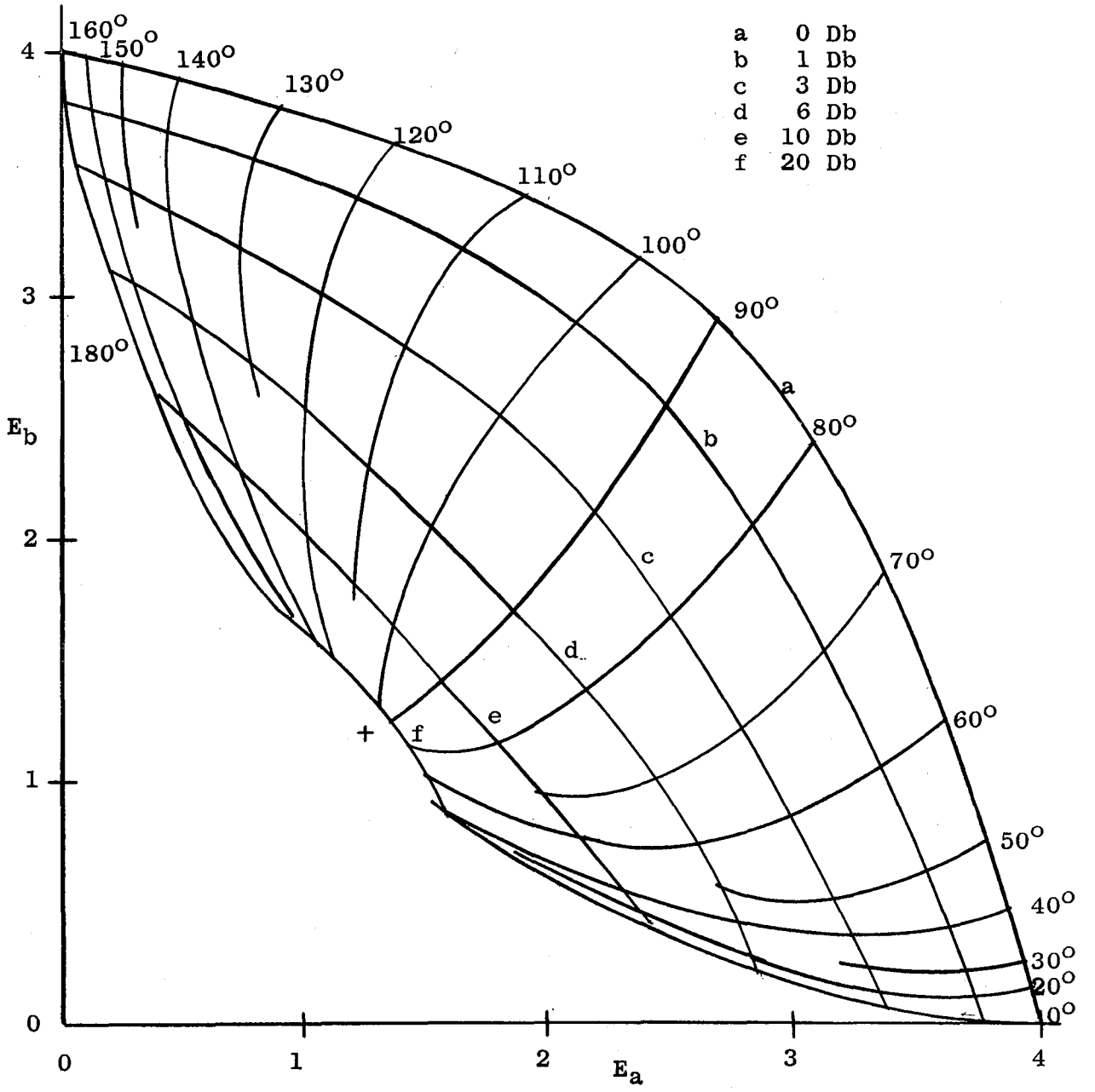

Units of E_a and E_b are "centimeters of oscilloscope deflection"

Fig. 8. Microwave bridge calibration.

One other consideration of the microwave circuit which must be taken into account is the heating of the electron gas by the alternating electric field of the microwave signal. Since the microwave signal is used as a diagnostic tool, its influence on the electron motion should be negligible. A criterion has been arrived at by V. E. Golant[31] by consideration of the change in mean electron energy due to the microwave field relative to the change in mean electron energy due to collisions with heavy particles. If the microwave field is to have a negligible effect, then the criterion may be stated mathematically as

$$\frac{1}{2}\frac{\sigma_r E^2}{n} \ll K_e \nu_m (W - W_t) \qquad (77)$$

where the term on the left represents the mean change in energy of an electron due to the microwave field and the right hand side represents the mean change in energy due to collisions with heavy particles. K_e is the effective energy transfer coefficient per collision, W is the mean electron energy and W_t is the mean energy of the heavy particles. If the real part of the conductivity is substituted in equation 77 and K_e is taken as 10^{-3} for a molecular gas[31], at 300° K the criterion reduces to

$$E \ll 2.1 \times 10^{-8} (\omega^2 + \nu_m^2)^{1/2} \text{ volts/meter} \qquad (78)$$

The experimental conditions are that $\nu_m \ll \omega$ and a frequency of 9180 megacycles was used. If these conditions are used in equation 78, it is found that the peak electric field intensity of the microwave signal should be much less than 1210 volts per meter. In X-band waveguide operating at a frequency of 9180 megacycles, this peak field corresponds to a power of 157 milliwatts for the TE_{10} mode of operation. The maximum microwave power passing through the plasma cell in any of the experiments was 5 milliwatts, which is less than 5% of this critical value.

D. Gated Radiometer - Temperature Measurements

The device employed for measurements of temperature in the

afterglow is a modified version of a Dicke comparison type radiometer[26]. Basically, the comparison type radiometer compares radiation from two sources and, through a null detection system, indicates when they are equal. If one source of radiation is a black-body radiating at a known variable temperature and the second source is a plasma, the radiometer may be employed to indicate when the two radiated powers are equal. As indicated in part II d, the radiation from a plasma is $B(\omega,T)\ A_\omega$, so it is then theoretically possible to calculate the temperature of the plasma if the absorption term A_ω is known. It was also pointed out in part II d (equation 62), that if the plasma were located between the standard and the radiometer, it would be possible to determine the plasma temperature without knowledge of the absorption term. Since an afterglow eventually disappears and the radiometer would then receive the radiation directly from the standard source, opportunity exists for switching the radiometer from the plasma to the standard by simply using a repetitive discharge of such a duration that the plasma decays completely in the first half of the discharge period. The details of this arrangement may be derived from consideration of Figures 9 and 10. Figure 9 is the microwave circuit consisting of (from the left) a termination; an argon discharge noise standard; a precision attenuator; the plasma cell; and the microwave receiver. The noise standard is essentially a black-body radiator at a known temperature T_s. The precision attenuator is at room temperature, T_o, and its attenuation, α_p, is accurately known. In the following discussion α is the attenuation ratio; i.e., α is equal to unity when there is no attenuation and to infinity when there is perfect absorption. Thus, the absorption term, A_ω, in equations 59 - 62 may be expressed as

$$A_\omega = 1 - \frac{1}{\alpha} \tag{79}$$

If the black-body radiation term $B(\omega,T)$ is expressed as its equivalent temperature, T, then by equation 60, the temperature equivalent of the microwave power at point T_1 in Figure 9 is

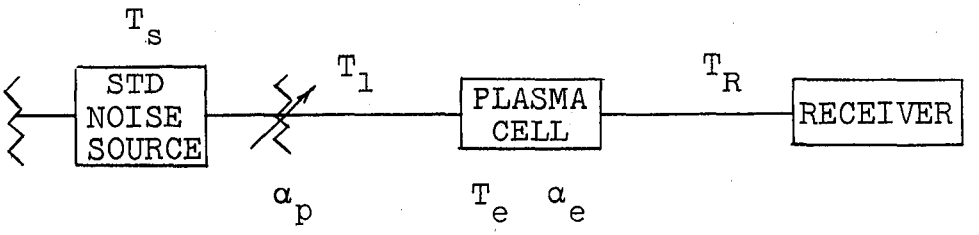

Fig. 9. Microwave circuit for temperature measurements.

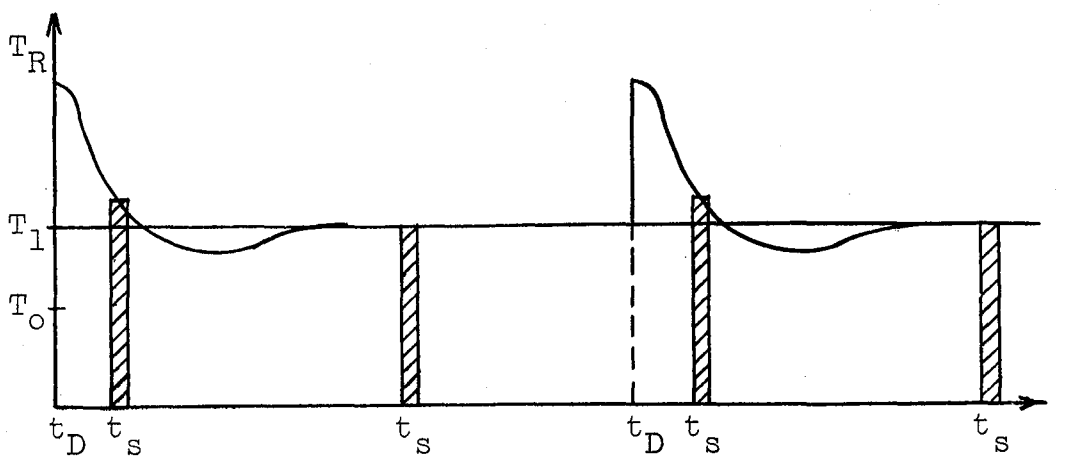

Fig. 10. Temperature measurements timing diagram.

$$T_1 = T_s \frac{1}{\alpha_p} + T_o \left(1 - \frac{1}{\alpha_p}\right) \tag{80}$$

Since all quantities on the right hand side of equation 80 are known and α_p is adjustable, then T_1 is a known variable temperature.

If the equivalent temperature of the electron gas in the plasma cell is T_e and the cell attenuation is α_e, the temperature equivalent of the microwave power "seen" by the receiver, T_R, is given by

$$T_R = T_1 \frac{1}{\alpha_e} + T_e \left(1 - \frac{1}{\alpha_e}\right) \tag{81}$$

The variation in time of T_R is sketched in Figure 10. The temperature and attenuation of the plasma cell rise rapidly during a short (5 microsecond) high voltage discharge (at T_D in Figure 10). The cell temperature, T_e, decays toward room temperature and by equation 81, T_R is approximately equal to T_e as long as the attenuation, α_e, remains appreciable. Then as the plasma disappears by recombination, etc., α_e approaches unity and T_R rises to the known standard level T_1. At the point where T_R decays through the known temperature T_1, equation 81 becomes

$$T_R \left(1 - \frac{1}{\alpha_e}\right) = T_e \left(1 - \frac{1}{\alpha_e}\right) \tag{82}$$

Thus at this point T_R is equal to T_e and is also equal to the known value T_1, irrespective of the value of the cell attenuation.

The discharge repetition rate is 100 cycles per second, which allows sufficient time for the plasma to decay in the first half of the period between discharges. The IF of the microwave receiver is gated on at a 200 cps rate at the times designated as t_s in Figure 10. The detected signal is the cross hatched pulses shown in Figure 10. The fundamental component of this pulse train is amplified in a high gain, narrow band, 200 cps amplifier and the result detected in a coherent phase detector.

The time between the discharge t_D and the sample t_s is

adjustable; thus measurements are made simply by setting t_s at a known time following the discharge and then adjusting the precision attenuator, α_p, until the microwave receiver indicates a null. T_e is then equal to T_1 and is given by equation 80.

The gate width of the receiver is adjustable with a minimum of 1 microsecond. The temperature sensitivity is approximately 10 degrees near room temperature, on the assumption that the plasma cell has an attenuation of at least 10 Db. during the instant of measurement. Meaningful measurements have been obtained with cell attenuations as low as 0.2 Db.

E. Spectrographic and Light Intensity Measurements

In addition to results obtained from microwave measurements of electron density and collision frequency, and measurements of the electron temperature, useful information may be obtained from the visible spectrum of the plasma. Both spectrographic measurements and total light intensity measurements were made.

Spectrographic measurements were made in nitrogen with a 3 1/4" by 4 1/4" Hilger quartz prism spectrograph. Originally it was intended to use the results of the spectrographic measurements to obtain information concerning the presence of the various molecular species of nitrogen, N, N_2, N_3, and N_4. The intent was to separate the bands of the different species by means of a Bausch and Lomb monochromator (after band location had been established spectroscopically) and to read out the band intensities of the separate species as a function of time in the afterglow by means of a photomultiplier tube. Experimentally, this measurement is not too difficult and preliminary results were obtained on the bands of N_2. This method was not pursued, however, since only bands attributed to N_2 were obtained. No lines or bands attributed to N, N_3 or N_4 were found. This method might be employed in other gases, where more than one molecular species is present.

Total light intensity measurements may be used to extend the range of electron densities obtained from the microwave method. In

the late afterglow, the radiation in the visible spectrum will be due to recombination of electrons and positive ions. Therefore the intensity, I, is proportional to the product of the electron and ion densities. If only one type of positive ion is present, the assumption of charge neutrality requires the electron density to equal the ion density, thus

$$I \quad \alpha \quad n_e^2 \tag{83}$$

The light intensity measurements are more sensitive than the microwave method. Thus the electron density-time data obtained from microwave measurements may be extended, using a photomultiplier to convert the light intensity to a voltage signal and applying this to an oscilloscope. The oscilloscope deflection will be proportional to the square of the electron density. The proportionality constant is obtainable from a calibration of the oscilloscope deflection at sufficiently high electron densities where the density may be obtained also by a microwave measurement. This method was successfully used to follow the electron density decay in the late afterglow. Because of the calibration problem and the fact that sufficient data could be obtained from the microwave interaction, this method was not pursued in the nitrogen experiments.

F. Outline of Experimental Procedure

The chronological order of experimental procedure and the description of experimental apparatus not covered elsewhere are described in this section. The first consideration is to use as pure a gas as possible. Therefore, before each experiment was begun, a new one liter flask of Linde MSC grade gas was attached to the vacuum system. The vacuum system was then baked at approximately 400° centigrade for at least 24 hours while pumping with a diffusion pump. Following the baking period, the closed system was pumped with a vacion pump to ultra-high vacuum pressures. During this pumping period the microwave hardware was assembled and the microwave bridge cali-

brated. If the vacuum system pressure rise was sufficiently slow in the absence of pumping to indicate no leakage and a "clean" system, the gas supply bottle was opened. The gas was then leaked into the vacuum system through a metal ultra-high vacuum valve.

In the calibration of the microwave bridge, the deflection of an oscilloscope signal corresponding to the detected output arm signals of the hybrid T detector is calibrated by the precision phase shifter and attenuator. A plot similar to Figure 8 is obtained where the units of the vertical and horizontal axes are "centimeters of oscilloscope deflection".

The plasma is formed in the plasma cell by means of a hard tube pulser. The total current is approximately 7 amperes and the duration is approximately 5 microseconds. Since the voltage drop in the cell is approximately 280 volts, approximately 10 millijoules of energy is imparted to the plasma in each breakdown pulse. The experiment is repeated every 10 milliseconds. Photographs are taken of the two hybrid T output arm signals and using the calibration curve, attenuation and phase shift of the microwave signal as a function of time in the afterglow is obtained. Electron density and collision frequency calculations were then performed on the IBM 650 computer using both equations 51 and 58. In equations 51 the assumption of a uniform spatial distribution of electron density was used, and in equations 58 the spatial distribution was assumed to be sinusoidal, corresponding to a diffusion controlled electron density decay. The data corresponding to equations 58 was used with equation 44 to determine the recombination coefficient and ambipolar diffusion coefficient. The data corresponding to equations 51 was used in the early afterglow, where recombination is predominant, to obtain the cross-section for momentum transfer.

The temperature measurements were carried out following the phase shift and attenuation measurements, since it was necessary to dismantle the microwave bridge and to set up the radiometer circuit shown in Figure 9. Care was taken to provide the same conditions as in the previous experiments. The pressure of the gas in the cell was reset to the values used in the bridge measurements. The hard tube pulser was also adjusted to give the same discharge conditions.

PART IV.

EXPERIMENTAL RESULTS

A. Introduction

In this section the results of measurements are presented. First, an ambipolar diffusion coefficient was obtained in helium. Since this gas has been studied in some detail in several laboratories, a check on the experimental method and apparatus is obtained. Detailed results of temperature and electron loss coefficient measurements in nitrogen are then presented. Finally, preliminary results of measurements of the cross-section for momentum transfer are presented. Discussion of results is deferred to part V.

B. Ambipolar Diffusion Coefficient in Helium

In order to obtain a check on the experimental method and apparatus, measurements of the ambipolar diffusion coefficient in helium were made. As stated above, helium gas has been studied in some detail in several laboratories[14, 35, 47].

The initial results for the ambipolar diffusion coefficient times pressure, $D_a p$, were scattered in the range 700 - 900 cm^2Torr/sec. A spectrographic study also showed the presence of an impurity taking an active part in the discharge. It might be pointed out that other investigators have also found it very difficult to obtain helium discharges free from impurity ions, owing to the high ionization potential of helium relative to the ionization potential of common impurities.

A cataphoresis pump[51] was added to the vacuum system in order to further purify the helium. The resultant value of $D_a p$ was 730 ± 50 cm^2 Torr/sec, which compares favorably with the value obtained by Kerr and Leffel[35] (700 cm^2 Torr/sec) in 1959 and the value obtained by Oskam[47] (665 ± 25 cm^2 Torr/sec) in 1957. In all of these cases, the helium molecular ion, He_2^+, is expected to be the predominant ion taking part in the ambipolar diffusion in the afterglow[48].

C. Results in Nitrogen

1. Temperature Measurements

The results of the temperature decay at various pressures

are shown in Figures 11 - 17. In all instances the time corresponds to the center of the receiver gate. The receiver gate widths used in obtaining each point are indicated at the top of each graph. The vertical limits on the plotted points give an indication of the sensitivity of the radiometer measurements. The standard noise source used was a TD-18 Bendix tube which has 15.83 Db excess noise, corresponding to a temperature of 11,390 degrees Kelvin.

Over the entire pressure range, the maximum time required for the electron temperature to relax to room temperature is 250 microseconds. The data used to obtain electron loss coefficients was therefore taken only at times longer than 250 microseconds.

In order to facilitate discussion in part V, a composite graph of the temperature decay for several pressures is plotted in Figure 18. In order to reduce confusion, the points which have a vertical range in Figures 11 - 17 have been plotted as a discrete point using the center temperature of the vertical range. Also, the abscissa is limited to the first 150 microseconds of the afterglow, since all curves are very close to each other following this time.

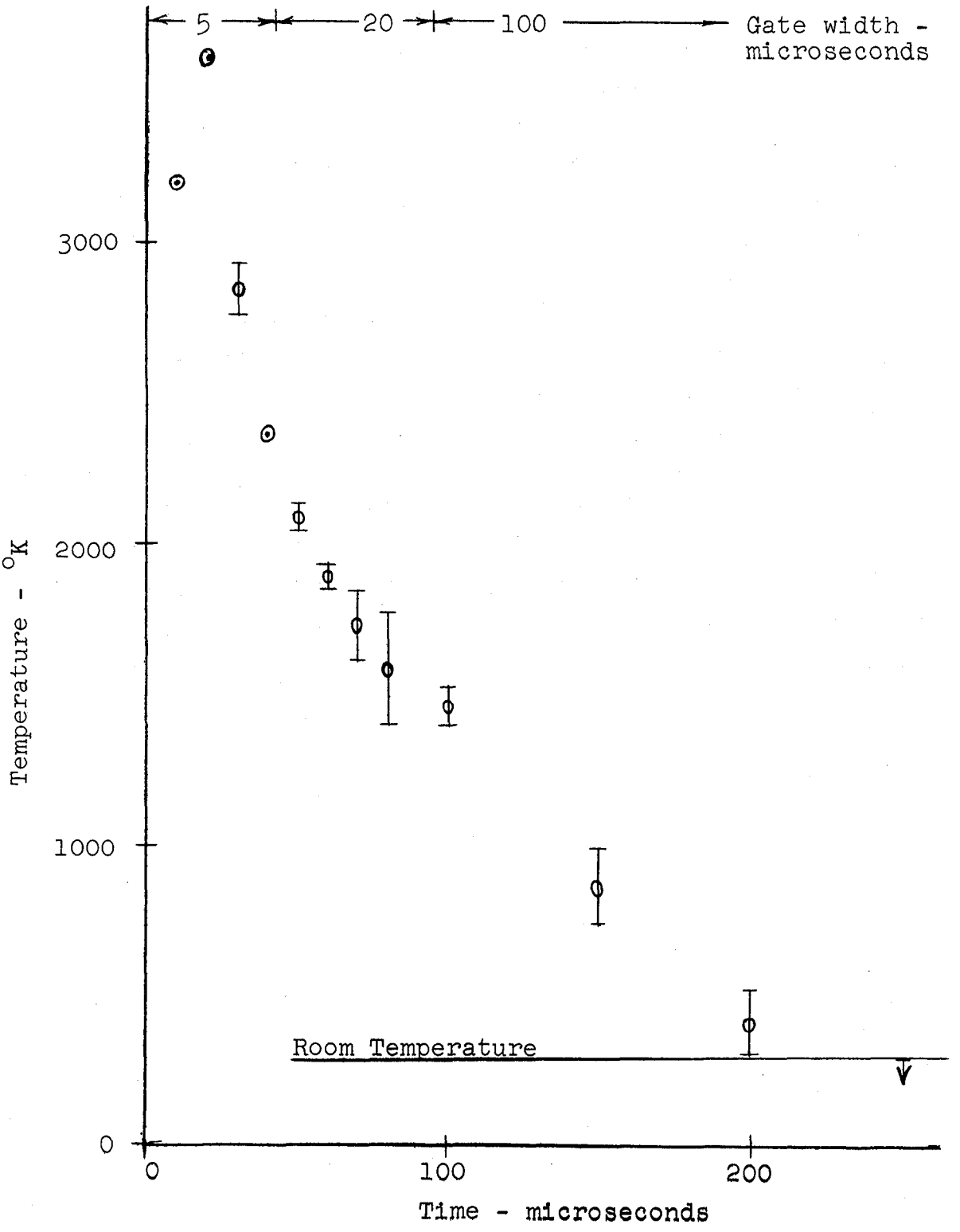

Fig. 11. Temperature decay at 7.1 Torr.

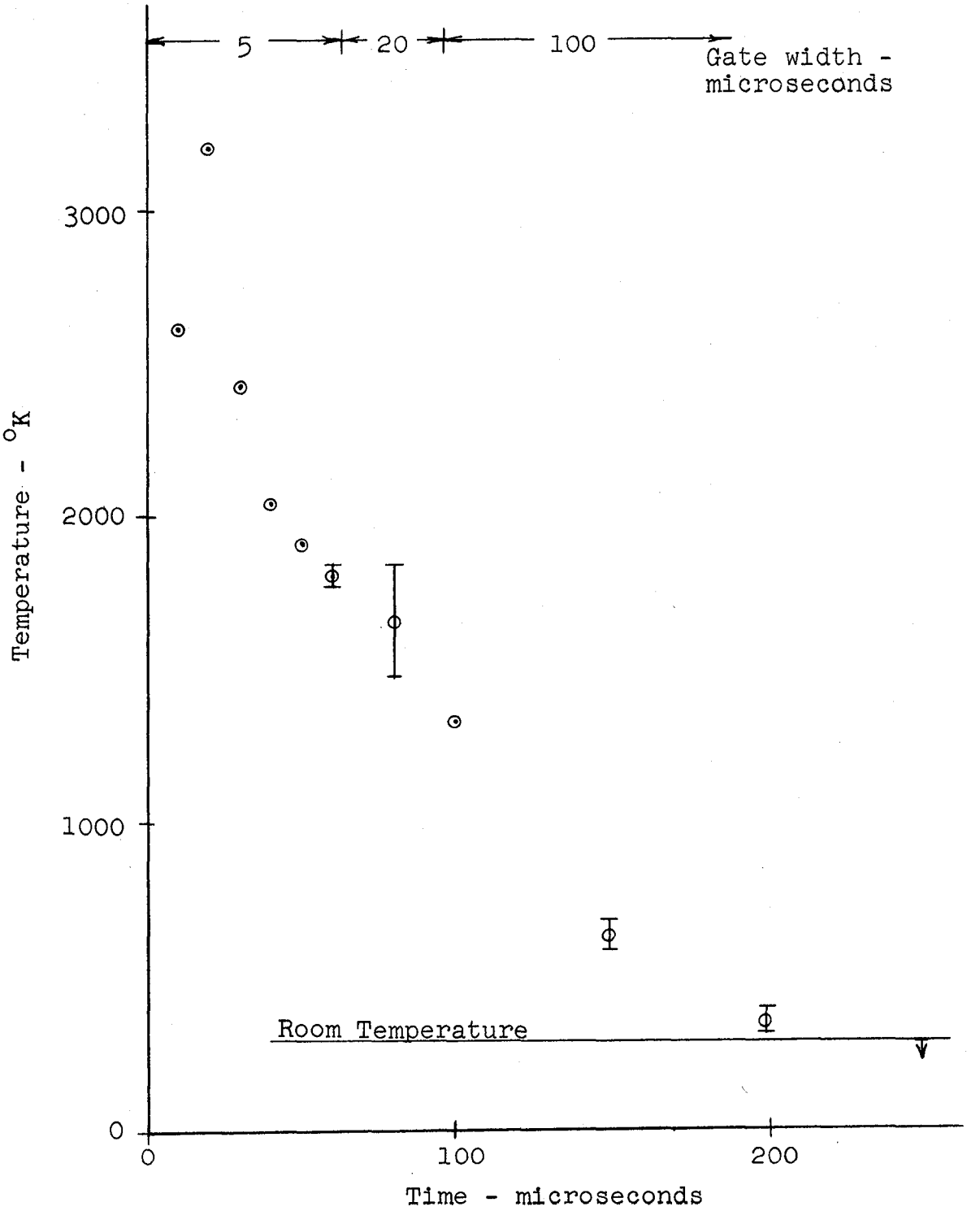

Fig. 12. Temperature decay at 4.6 Torr.

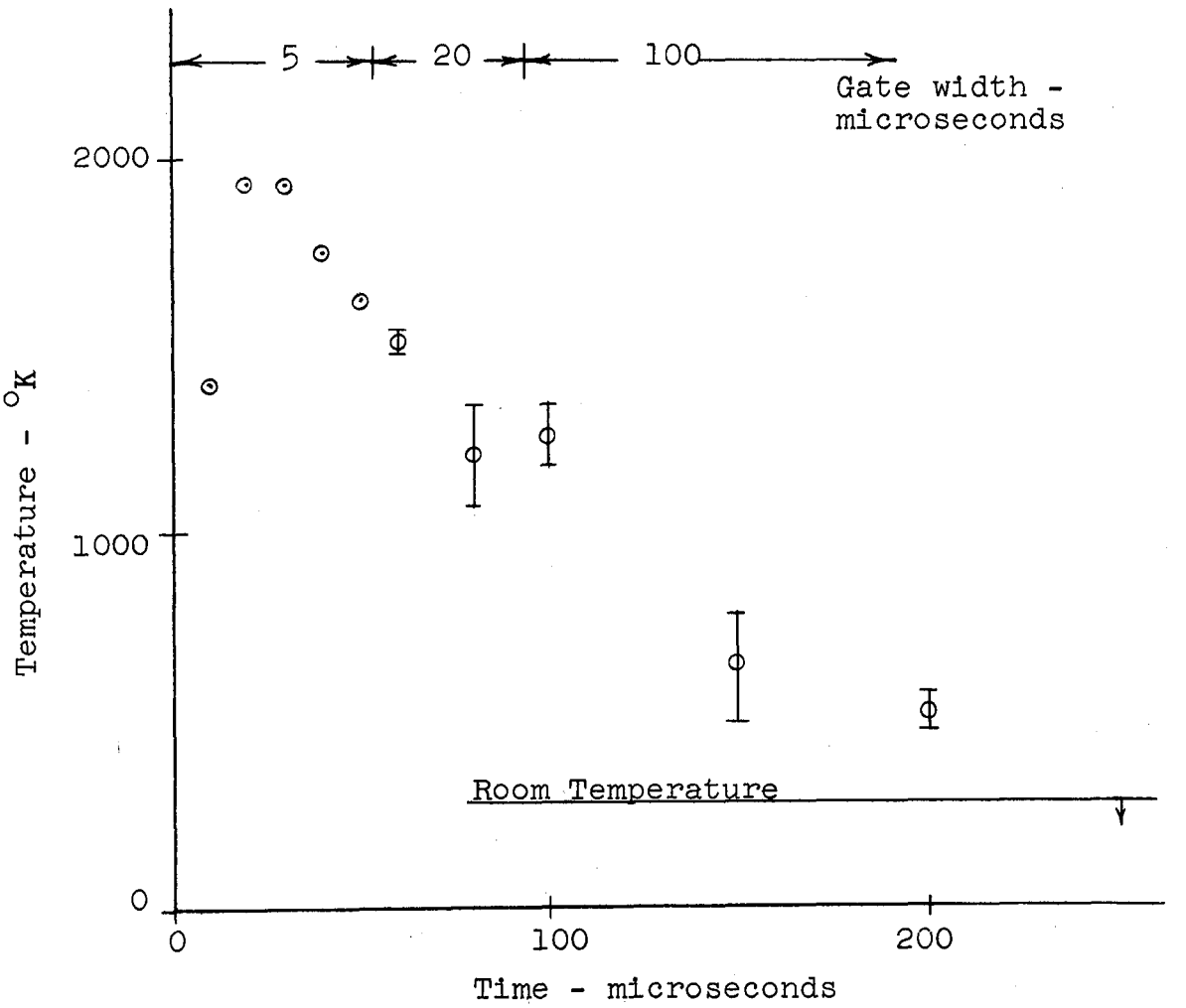

Fig. 13. Temperature decay at 2.95 Torr.

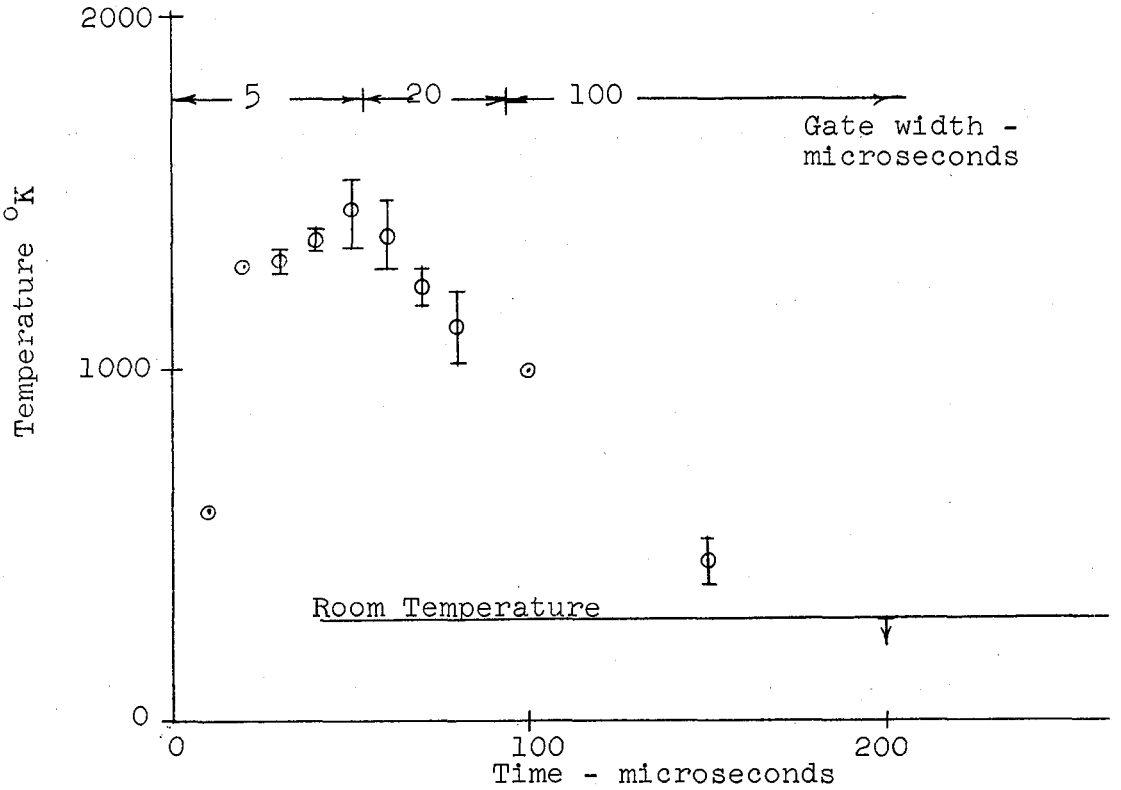

Fig. 14. Temperature decay at 1.95 Torr.

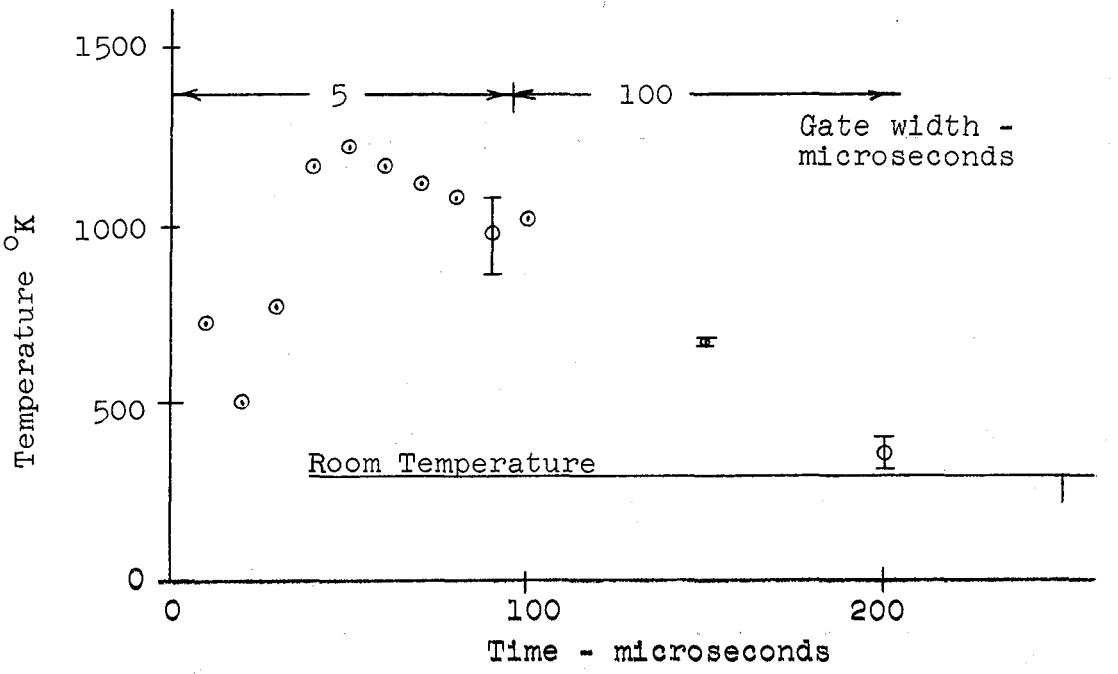

Fig. 15. Temperature decay at 1.2 Torr.

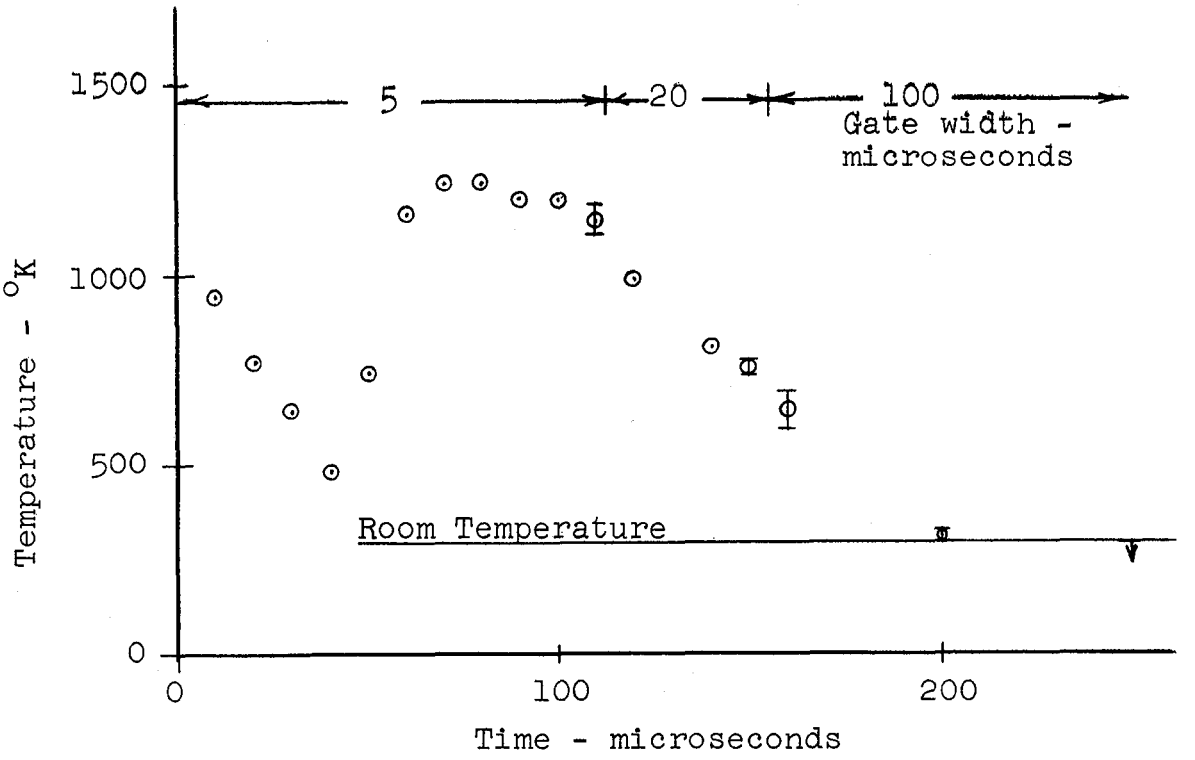

Fig. 16. Temperature decay at 0.75 Torr.

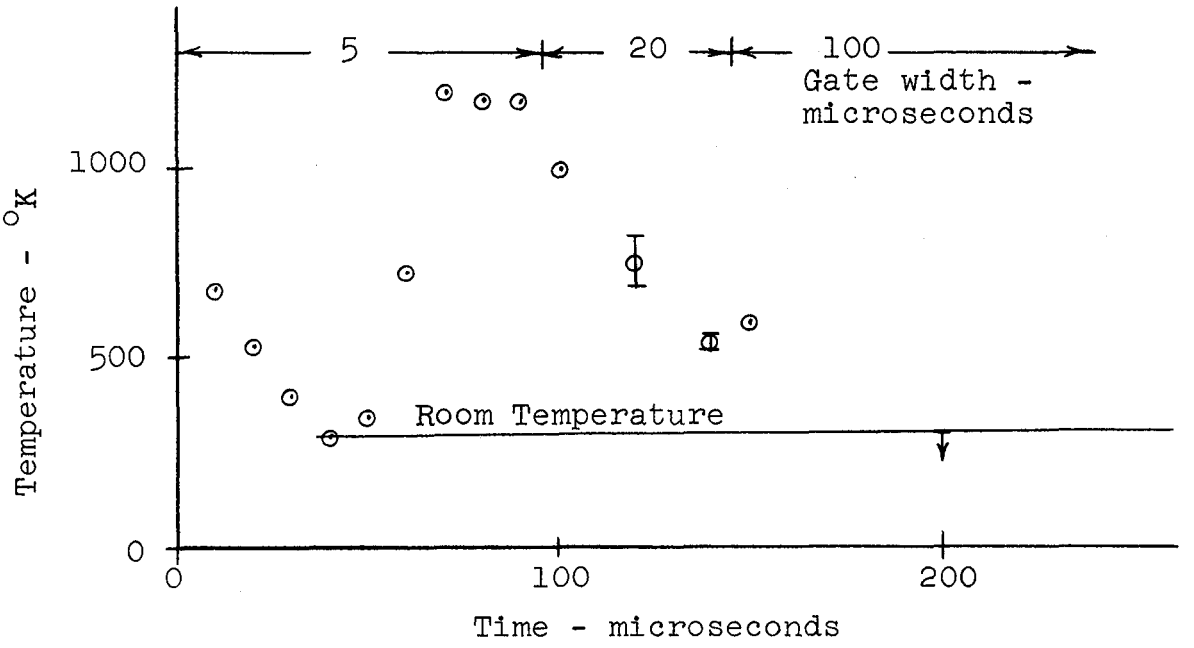

Fig. 17. Temperature decay at 0.45 Torr.

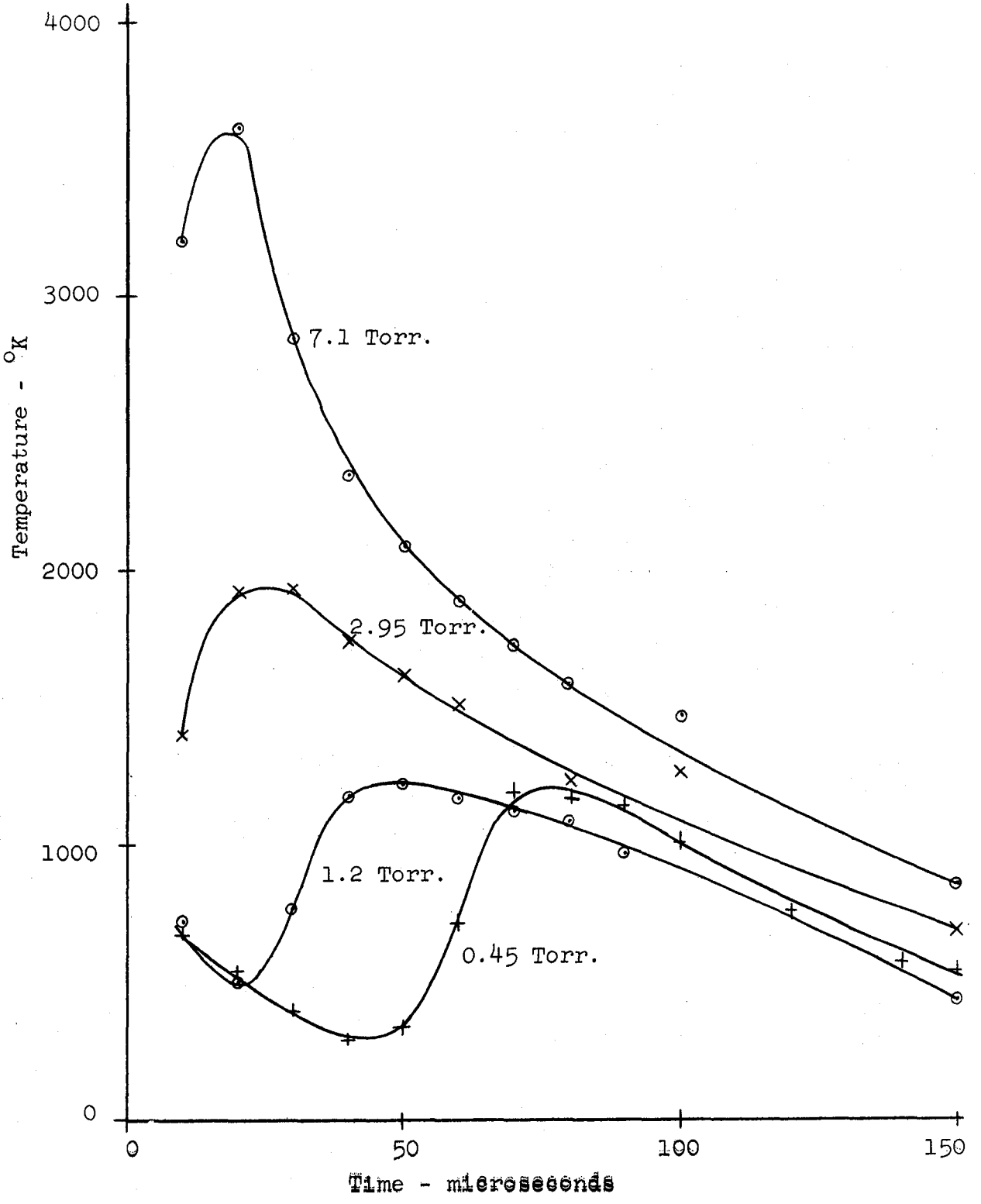

Fig. 18. Composite temperature decay.

2. Electron Loss Coefficients

It might be advantageous at this point to summarize the steps taken to obtain the ambipolar diffusion coefficient and recombination coefficient. Photographs were taken of the oscillograph traces of the hybrid T detector output signals. The photographic negatives were placed in an enlarger so the curves could be traced directly onto graph paper. Thus E_a and E_b (Figures 7 and 8) were obtained as a function of time. At specific times the attenuation and phase shift of the microwave signal were obtained from the calibration curve (Figure 8). Time increments of 10 microseconds were used in the early afterglow where the electron density is changing rapidly and a 50 microsecond time interval was used in the late afterglow. The values of attenuation, phase shift, and the corresponding time were then tabulated and punched onto IBM cards. The electron density and collision frequency were calculated by machine (IBM 650) employing equations 58 and the time corresponding to each calculation was transferred to the answer card. The computer thus furnished tabulated values of electron density, collision frequency and time.

The incremental changes in electron density and time were then computed. The computed results were used to obtain values for the left hand side of equation 44

$$\frac{1}{n_o}\quad\frac{\Delta n_o}{\Delta t} = -k - \alpha n_o \tag{44}$$

and the left hand side of equation 44 was plotted as a function of n_o. k and α were obtained from the intercept and slope of the resultant straight line by the method of least square deviation. D_a was then found from k by the relation

$$k = D_a \pi^2 \left(\frac{1}{a^2} + \frac{1}{b^2} + \frac{1}{c^2} \right)$$

As a check on the results, k and α were substituted into equation 42.

$$n_o(t) = \frac{C_1 k e^{-kt}}{1 - \alpha C_1 e^{-kt}} \qquad (42)$$

where

$$C_1 = \frac{n_o(o)}{k + \alpha n_o(o)}$$

C_1 was obtained from one of the data points and the value of n from equation 42 was plotted on the same graph as the data points. The resultant graphs are shown in Figures 19 - 26. In these figures the solid line is n versus t from equation 42. The points are the actual data points and the dashed line is the density decay assuming loss by the fundamental diffusion mode. The dashed line is the asymptote of the solid curve. The difference between the dashed line and solid curve is the effect of the recombination in equation 42. In the early period immediately following the discharge, it is expected that the solid curve will deviate from the data points due to losses in higher order diffusion modes and to changes in the recombination coefficient and the ambipolar diffusion coefficient, the loss coefficients in general being temperature dependent.

The values of the constants used in equation 42 and the ambipolar diffusion coefficients obtained are shown on each of the Figures 19 - 26. The results of the ambipolar diffusion coefficient times pressure, $D_a p$, are plotted as a function of pressure in Figure 27. The average value of $D_a p$ at pressures below 4.6 Torr is 123 cm^2 Torr sec^{-1} with a spread of $\pm$ 24 cm^2 Torr sec^{-1}. The point at 7.1 Torr is extremely high, which may be due to the fact that at this high pressure diffusion loss is small compared to the recombination loss. The method employed to obtain the diffusion coefficient is relatively insensitive at this high pressure.

The results for the recombination coefficient are shown in Figure 28. It is noted that the recombination coefficient increases with pressure initially, and tends to level out at high pressures at approximately 7×10^{-7} cm^3 sec^{-1}. These results will be discussed further in part V.

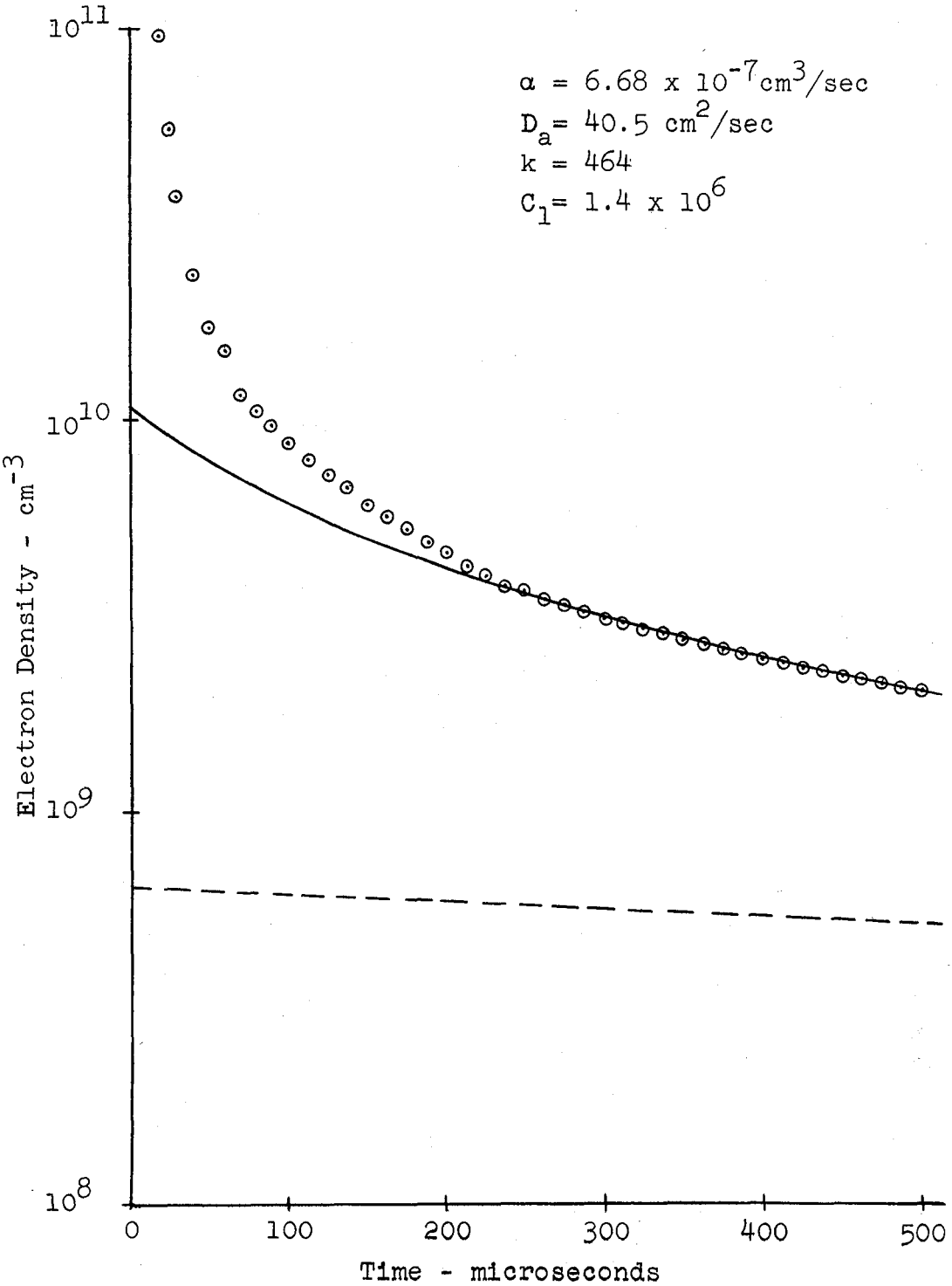

Fig. 19. Electron density as a function of time at 7.1 Torr.

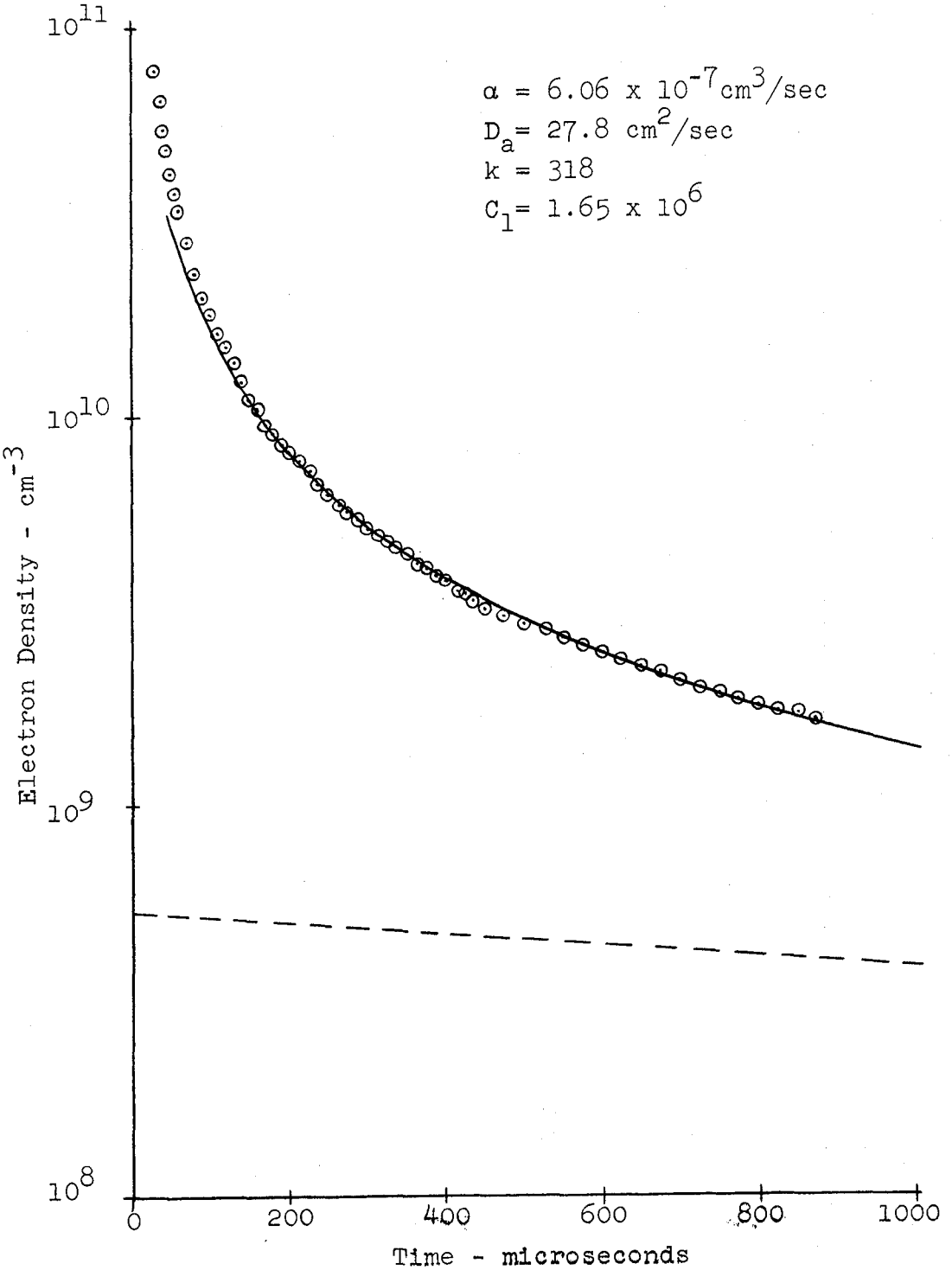

Fig. 20. Electron density as a function of time at 4.6 Torr.

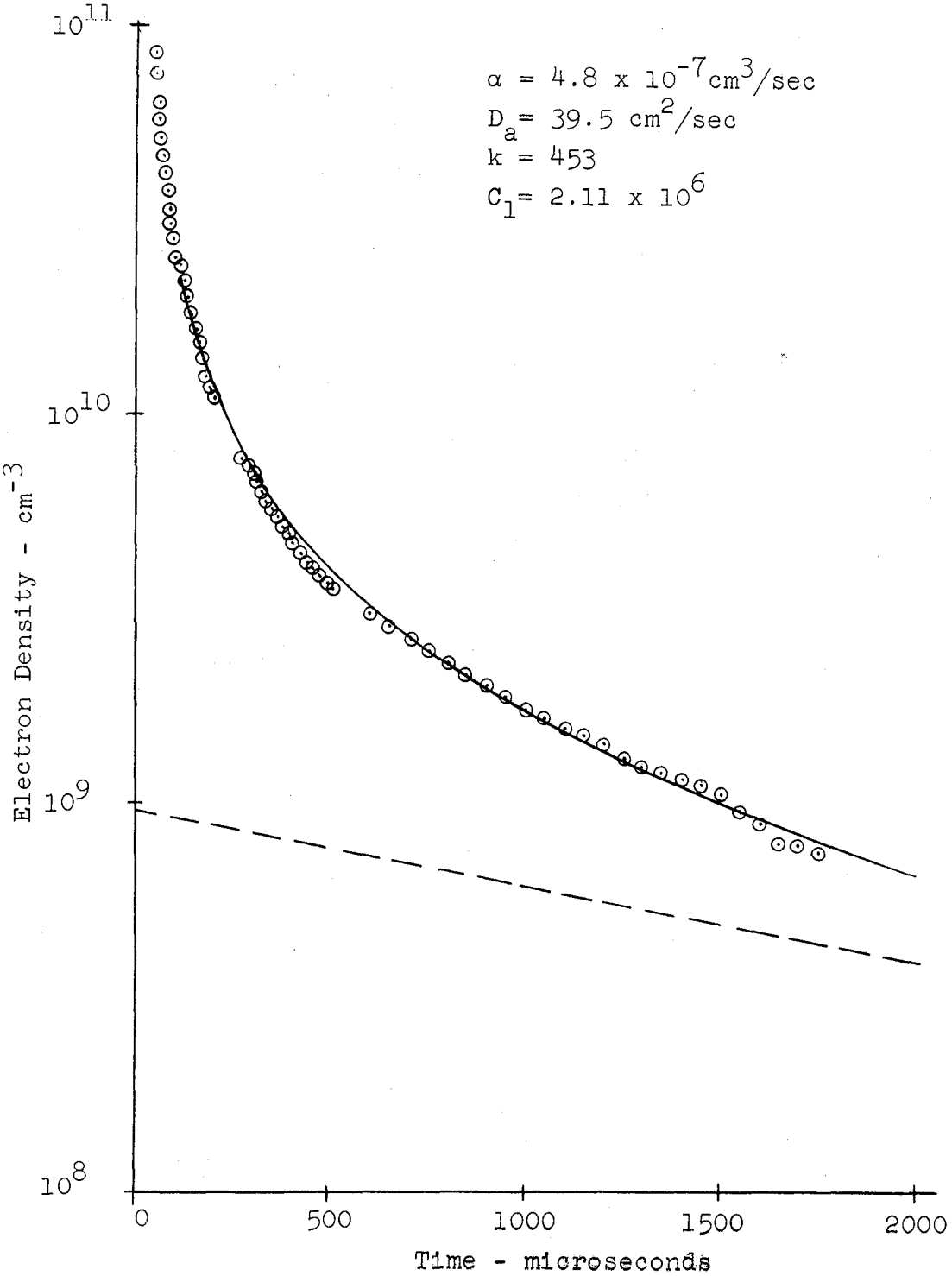

Fig. 21. Electron density as a function of time at 2.95 Torr.

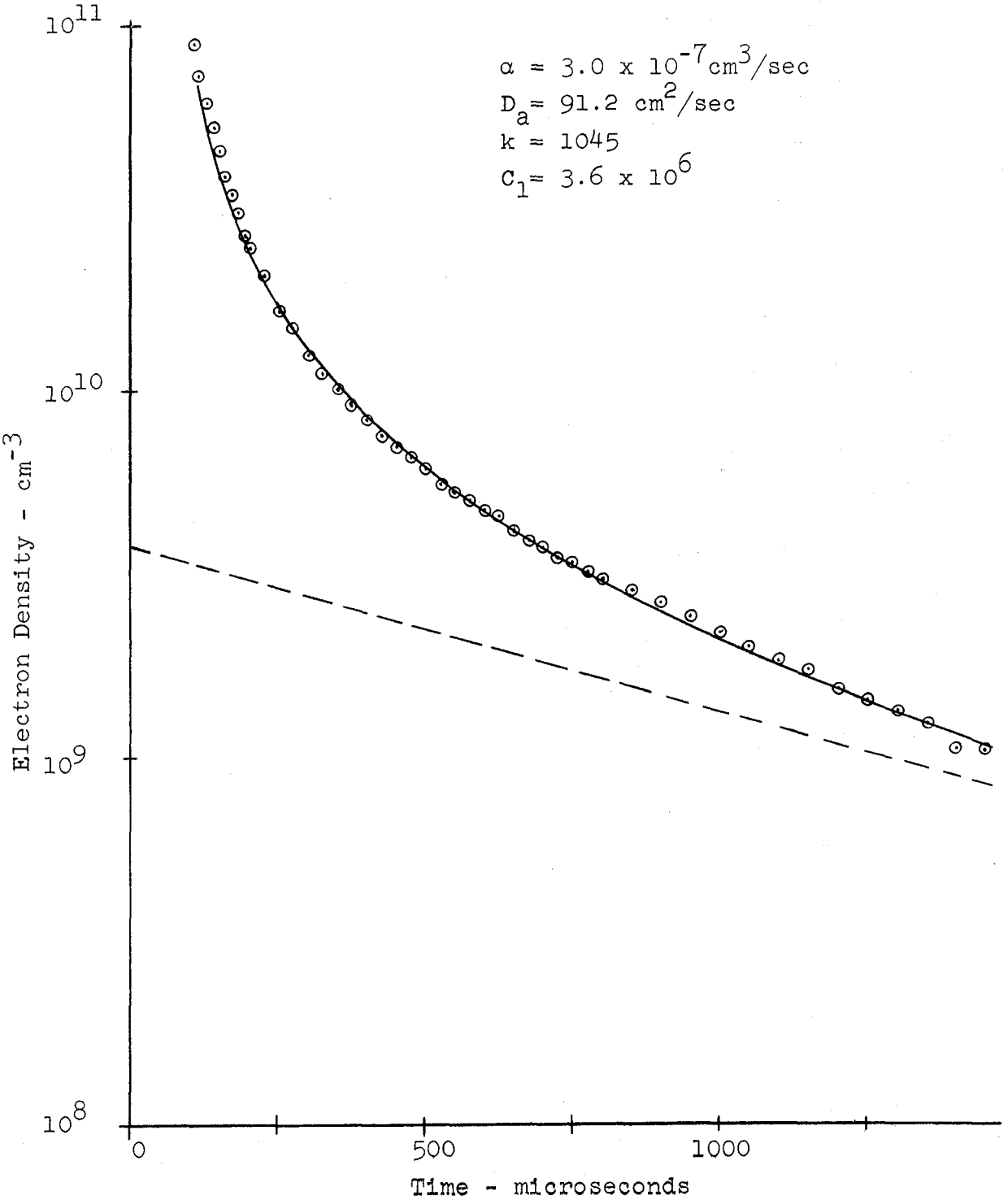

Fig. 22. Electron density as a function of time at 1.2 Torr.

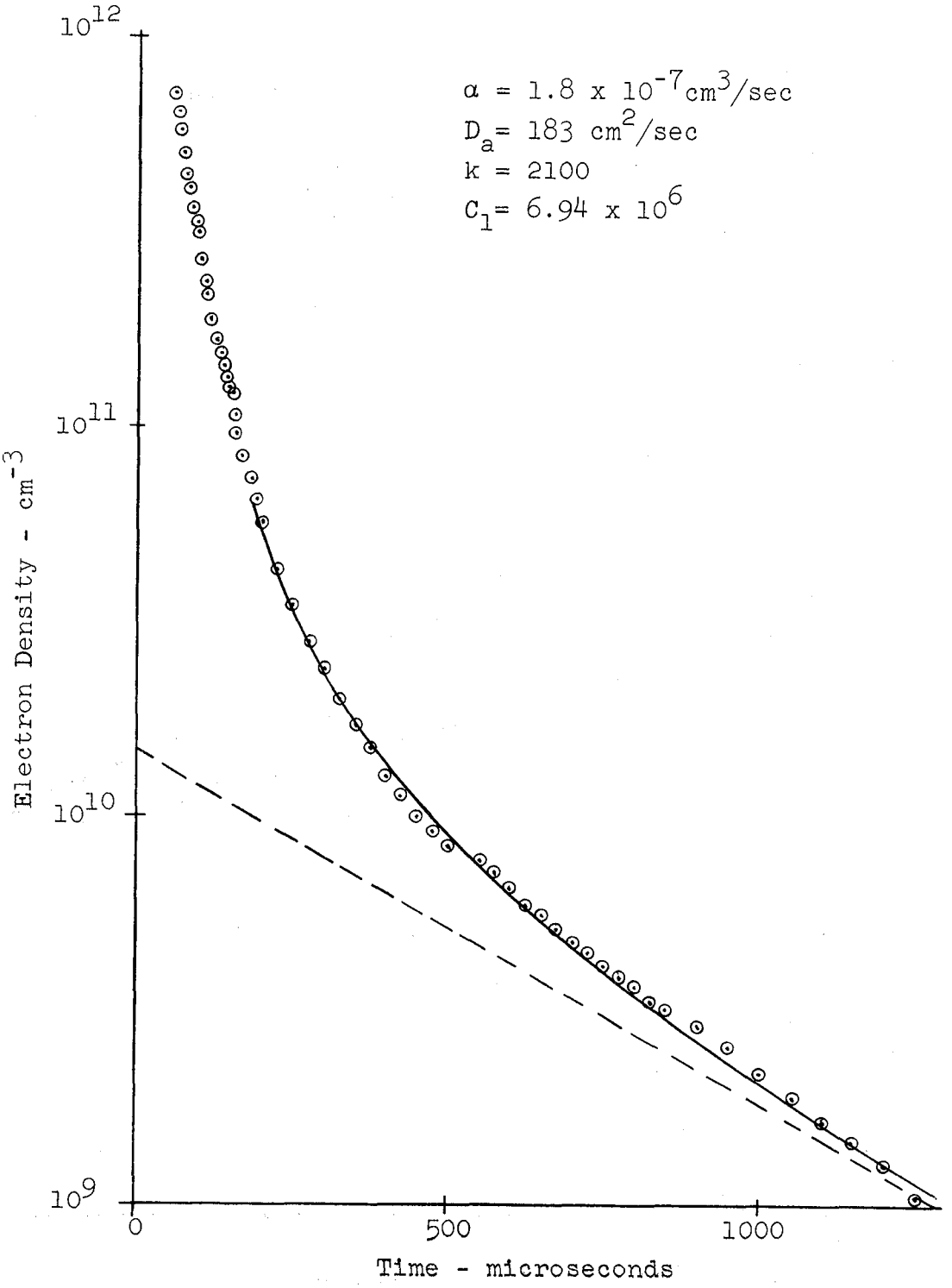

Fig. 23. Electron density as a function of time at 0.75 Torr.

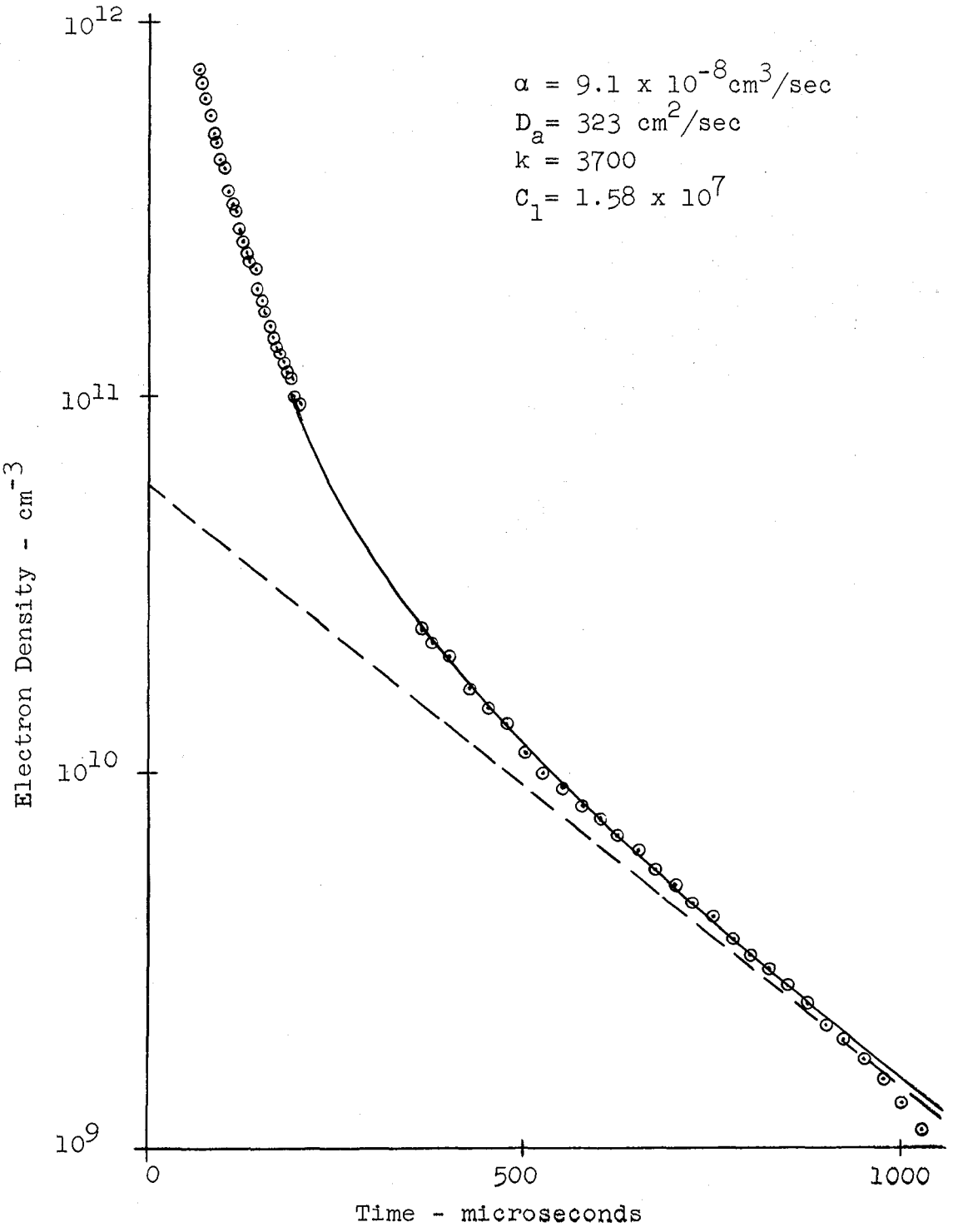

Fig. 24. Electron density as a function of time at 0.45 Torr.

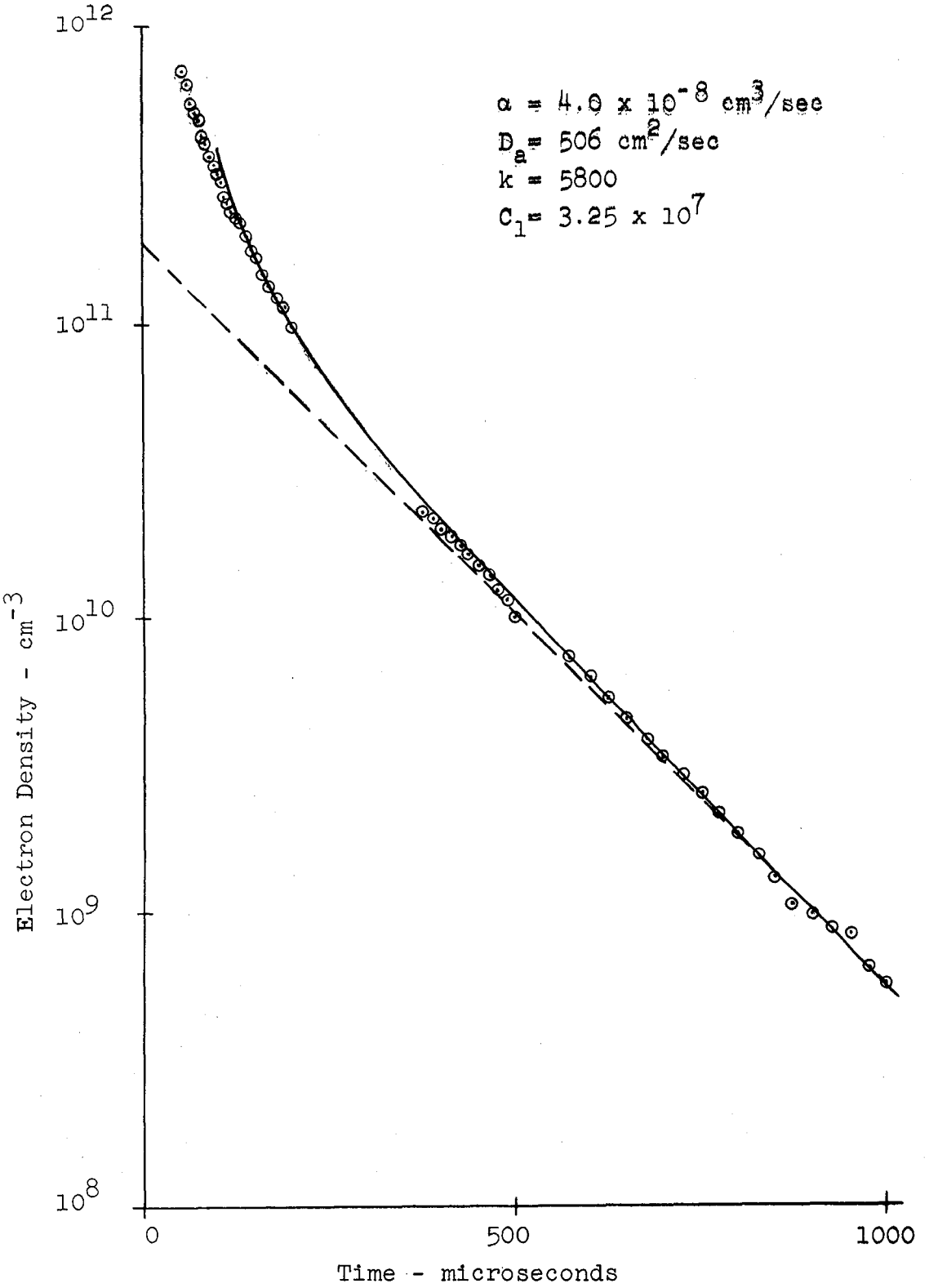

Fig. 25. Electron density as a function of time at 0.25 Torr.

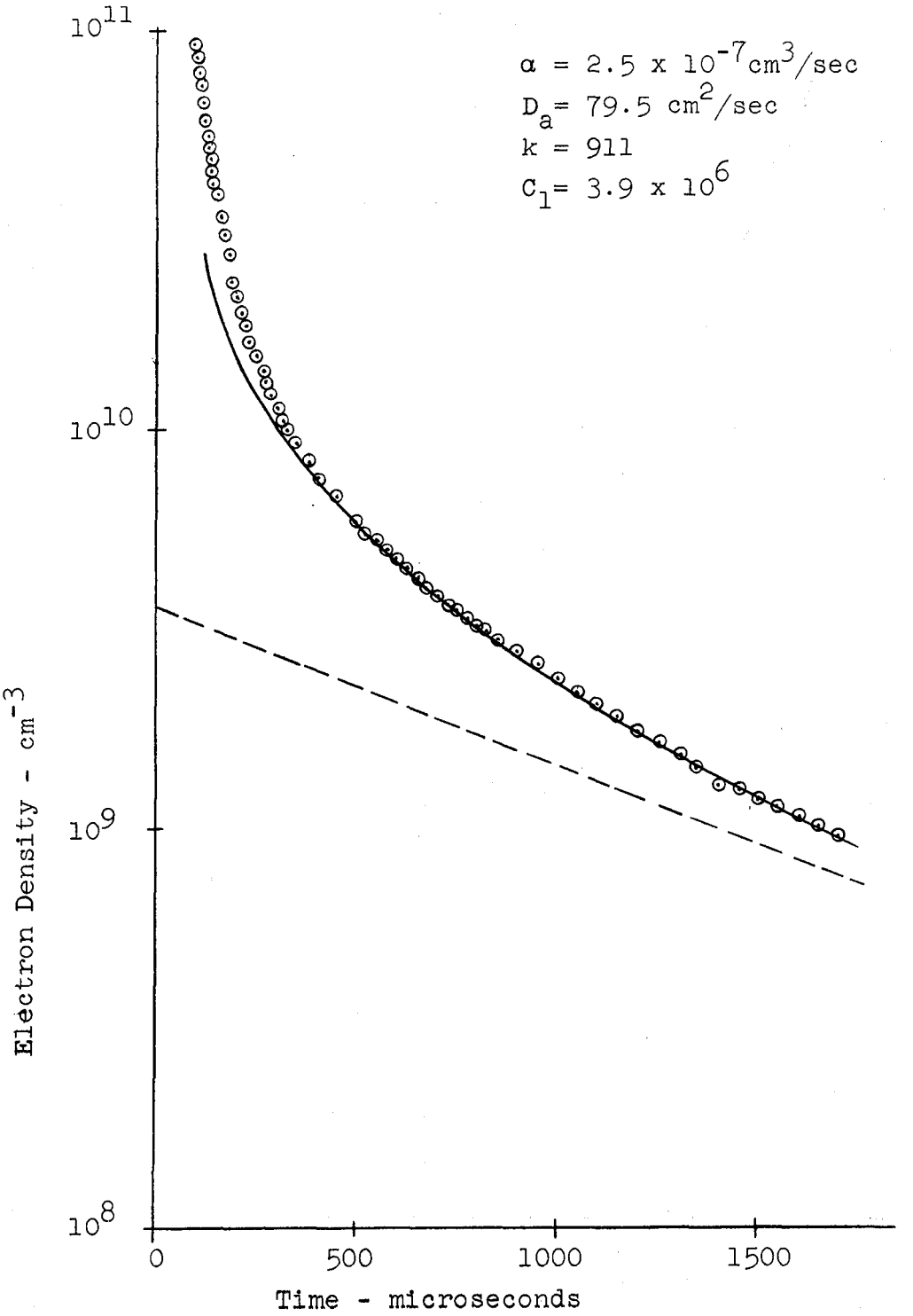

Fig. 26. Electron density as a function of time at 1.25 Torr.

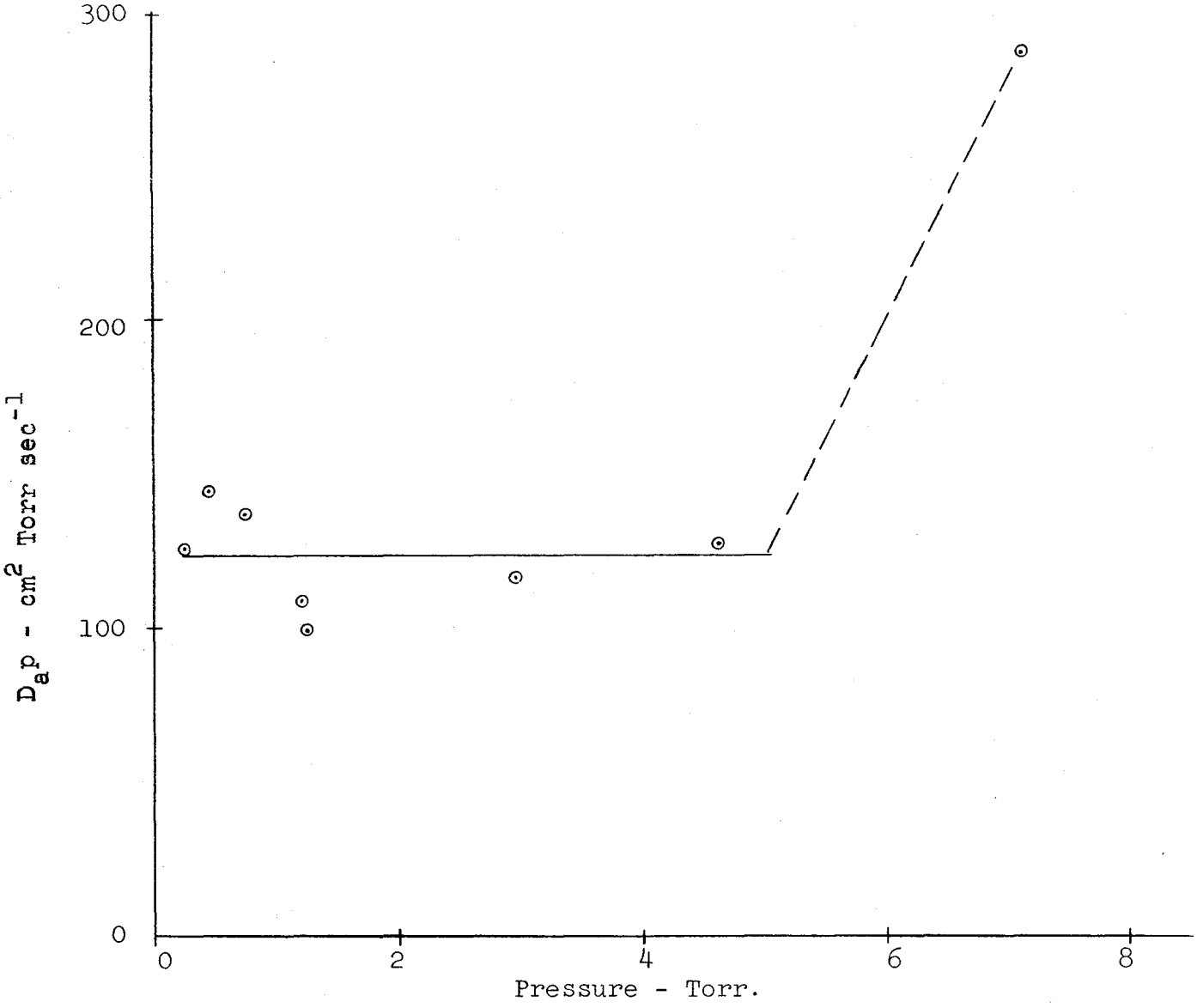

Fig. 27. $D_a p$ as a function of pressure.

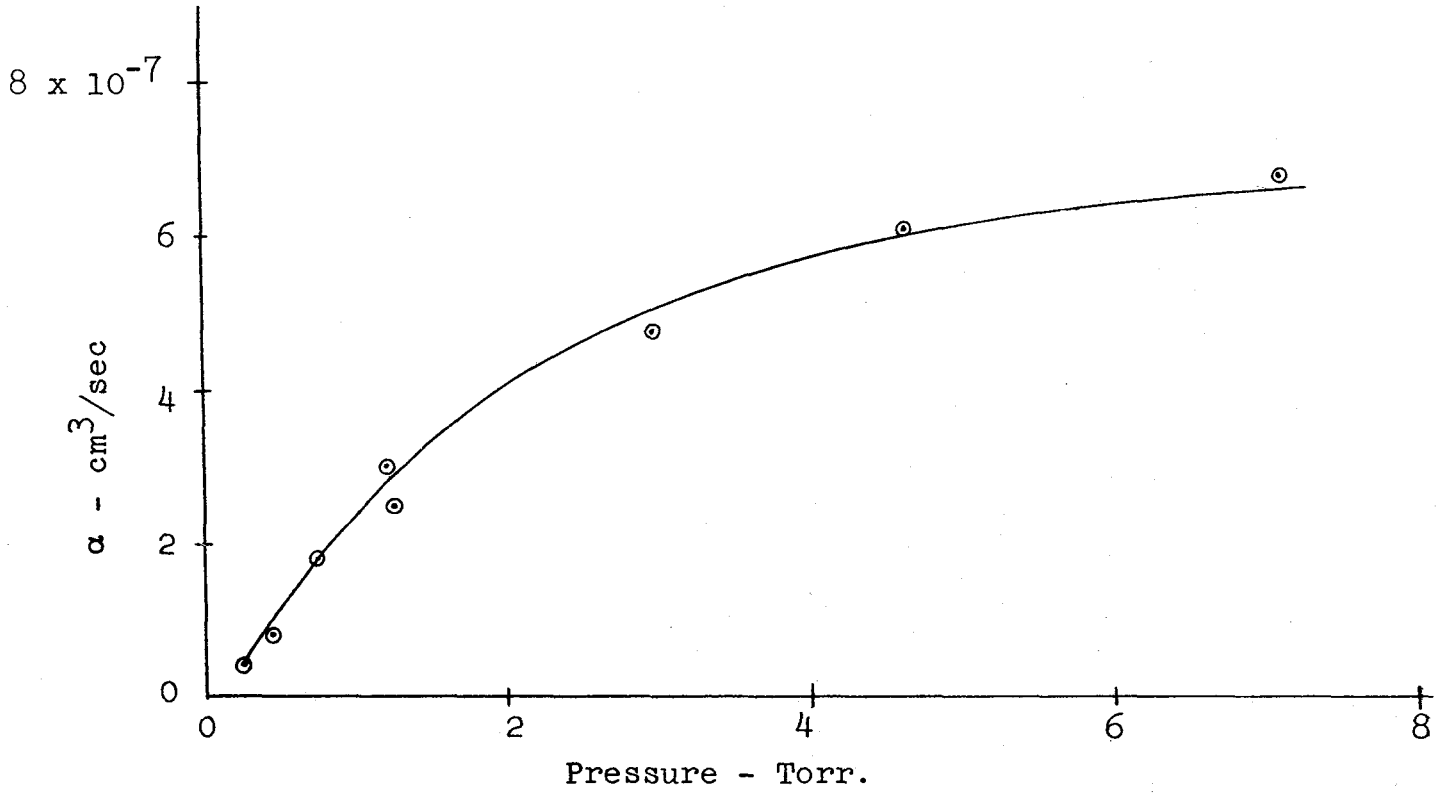

Fig. 28. Recombination coefficient as a function of pressure.

3. Cross-section for Momentum Transfer

Preliminary results have been obtained for the cross-section for momentum transfer. The results shown in Figure 29 were taken at two values of pressure, 7.1 and 4.6 Torr. The points obtained at 7.1 Torr are widely scattered, and the results obtained at 4.6 Torr are but slightly better.

The method used was to calculate the cross-section from the measured value of collision frequency as outlined in part II E. The scatter of points can be attributed to the lack of sufficient accuracy in the attenuation measurements which were used to calculate the collision frequencies. The primary concern was to obtain accurate electron densities in order to calculate electron loss process coefficients. The electron density depends primarily on the phase shift and it is insensitive to changes in attenuation in the late afterglow. Therefore, no attempt was made to obtain attenuation more accurately than the values obtainable from the hybrid T characteristic (Figure 8). In equation 51, however, it is noticed that the collision frequency is directly proportional to the attenuation. In order to reduce the scatter of points, more accurate measurements of attenuation would have to be made. All values shown in Figure 29 are within a factor of two of results obtained by other methods.

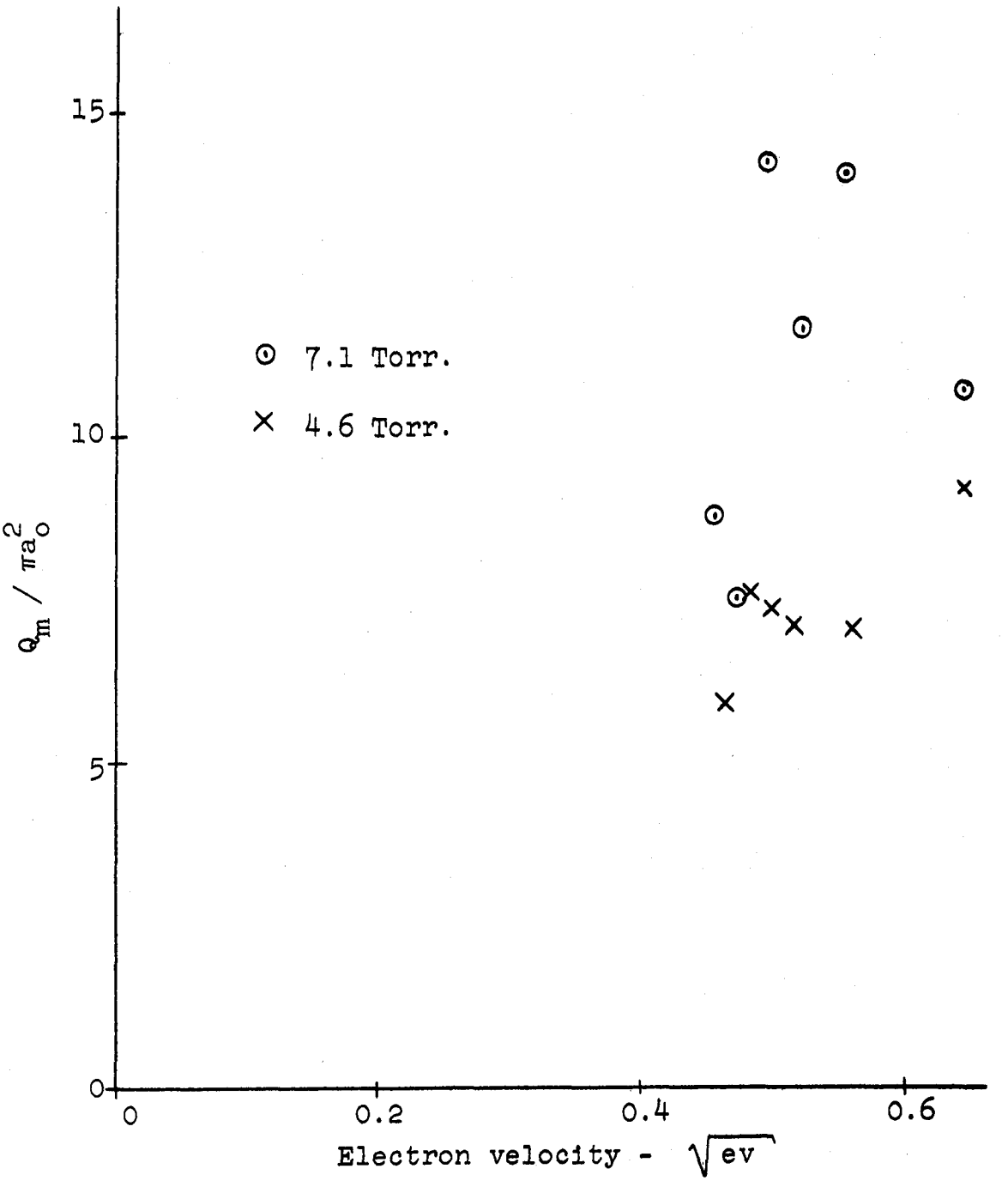

Fig. 29. Cross-section for momentum transfer.

PART V.

DISCUSSION OF RESULTS

The results for the recombination coefficient differ markedly from previous measurements using the guided transmission technique by Bialecke and Dougal[13]. In their measurements reported as 300° K, the recombination coefficient was found to be approximately 9.0×10^{-7} cm^3/sec independent of pressure in the range 0.2 to 2 Torr. However, in their work they allowed only 50 microseconds for the electron temperature to relax to room temperature following the discharge, and the data were taken for only approximately 200 microseconds following the discharge (see Figure 2, reference 13). On comparing these time values with the results of temperature measurements (Figures 11 - 17), we see that Bialecke and Dougal took their data when the electron temperature was much higher than room temperature. They also found that the recombination coefficient decreased with increasing temperature. One would expect then that their measured value of recombination coefficient would be lower than the value at 300°K. That this is not true may be explained as follows. They used a linear plot of $1/n_e$ as a function of time and obtained the recombination coefficient from the slope, neglecting electron loss by diffusion entirely. Gray and Kerr[32] have done extensive work examining the reliability of results for the recombination coefficient based on $1/n_e$ vs. time plots. They have concluded that one cannot deduce a reliable recombination coefficient from a plot of $1/n_e$ vs. time, even though it may be linear, unless the range of electron densities involved covers at least an order of magnitude, and that in general the method yields too high a value of the recombination coefficient. Since Bialecke and Dougal obtained linear plots of $1/n_e$ vs. time for only a factor of three or four in electron densities, the results should be viewed with extreme caution. One additional point--Bialecke and Dougal have attributed recombination to the dissociative recombination via N_2^+ according to the reaction

$$N_2^+ + e^- \rightarrow N^* + N^*$$

where the asterisk denotes excited atoms. Such a reaction would result

in spectra of atomic nitrogen, but as stated in the results section of this present work, only spectra attributed to the molecule N_2 were found. In a spectrographic study by Bryan, Holt and Oldenberg[21], lines attributed to atomic nitrogen were never observed in the afterglow over the pressure range of 3 - 30 Torr.

It is therefore important to point out that, although the microwave technique is a powerful diagnostic tool, other types of measurements are necessary to complete the description or to clarify the questionable assumptions of afterglow studies.

Other measurements of the recombination coefficient in nitrogen were the following. Biondi and Brown[15] made the first microwave determinations in 1949, using a cavity method, and obtained 14 x 10^{-7} to 18 x 10^{-7} $cm^3/sec.$ at pressures between 5 and 10 Torr. Their data were not corrected for diffusion loss. Faire and Champion[28] in 1959 obtained a value of 4 x 10^{-7} $cm^3/sec.$ at 4 Torr, which is in good agreement with the present work. They used the cavity method and corrected their data for diffusion loss. A value of 14 x 10^{-3} $cm^3/sec.$ was obtained before corrections for diffusion were made. This is precisely the value obtained by Biondi and Brown. Quite recently Kasner, Rogers, and Biondi[34] used a cavity technique and, in addition, a Boyd type[16] rf mass spectrometer for ion identification. They also used an inert buffer gas (helium or neon) to inhibit particle loss by diffusion. In this way they were able to measure recombination coefficients at low partial pressures of nitrogen, where ordinarily diffusion would be the principal electron loss mechanism. The value of recombination coefficient found for N_2^+ at partial nitrogen pressures of approximately .005 Torr was 5.9 $\pm$ 1 x 10^{-7} $cm^3/sec.$ A significant result of their work is the fact that at nitrogen pressures of 0.1 to 7.0 Torr the predominant afterglow ions were N_3^+ and N_4^+. It was only at nitrogen pressures less than .01 Torr that N_2^+ was found to be the only significant ion in the afterglow. This fact will be discussed further in attempting to describe the afterglow process.

Possible recombination processes in nitrogen are:

(1) $N_2^+ + e^- \rightarrow N_2 + h\nu$ radiative

(2) $N^+ + e^- \rightarrow N + h\nu$ radiative

(3) $N^+ + e^- + N_2 \rightarrow N^* + N_2$ 3-body collisional

(4) $N_2 + N_2^+ \rightarrow N_4^+$

$N_4^+ + e^- \rightarrow N_2 + N_2^*$ 2-step dissociative

(5) $N_2^+ + e^- + N_2 \rightarrow N_2 + N_2^*$ 3-body collisional

(6) $N_2^+ + e^- \rightarrow N^* + N^*$ dissociative

Reactions 2, 3 and 6 are eliminated because the spectrum of atomic nitrogen could not be found in the afterglow. In an article by Massey[45] in which extensive theoretical work on recombination is reviewed, it is shown that the radiative recombination coefficient is expected to be less than 10^{-11} cm^3/sec. Therefore reaction 1 above cannot produce the results of the present experiment. In the same paper[45] the three-body recombination coefficient for air "might be as large as $2 \times 10^{-10} p$ cm^3/sec." (p is the pressure in Torr). If the recombination coefficient for pure nitrogen is within an order of magnitude of this value, the results of the present experiment are three orders of magnitude higher than the expected value for three-body recombination. Therefore reaction 5 is not likely.

Bates[9] has shown that dissociative recombination is likely to occur faster than other processes; recombination coefficients in the order of 10^{-7} cm^3/sec. are made likely in this way. This is the reason that Bialecke and Dougal chose reaction 6 to explain their measured values. However, since only N_2 spectra are found in the afterglow, it is more likely that reaction 4 is predominant. This theory is also substantiated by Biondi's work with the mass spectrometer showing N_4^+ ions outweighing the population of the N_2^+ ion in the pressure range of these experiments.

Varney[54] in 1953, while studying drift velocities in nitrogen, obtained two distinctive regions in plots of drift velocity vs. E/p which he attributed to the presence of the N_2^+ ion at high E/p values (low pressure) and N_4^+ ion at low E/p values (high pressure). This attribution was strengthened in 1957[55] when he studied the temperature dependence of the drift velocities. He found that higher temperatures cause onset of the transition from N_4^+ to N_2^+ at lower E/p values. This change is in accordance with the belief that as impacts between ions and gas molecules grow more energetic, the N_4^+ ions should dissociate and travel at the speed characteristic of N_2^+ ions. He has shown that the reversible reaction

$$N_2^+ + N_2 \rightarrow N_4^+ \qquad (84)$$

$$N_4^+ + N_2 \rightarrow N_2^+ + 2N_2$$

favors the presence of N_4^+ at higher pressures and N_2^+ at lower pressures (no specific pressure values given).

From these facts, the recombination process in this present work is believed to be predominantly

$$N_4^+ + e^- \rightarrow N_2 + N_2^* \qquad (85)$$

The rate of this reaction would be expected to depend on the pressure, since according to equation 84 the presence of N_2 molecules is required to form the N_4^+ ion. The question is not entirely answered, however, since the 3-body reaction

$$N_2^+ + e^- + N_2 \rightarrow N_2^* + N_2 \qquad (86)$$

although considered unlikely by Massey, is not entirely ruled out. Spectra would again show only N_2 lines and the process is pressure dependent. The recombination process may be a mixture of the pro-

cesses described by equations 85 and 86 changing as a function of pressure as the relative populations of N_2^+ and N_4^+ are varied. Perhaps an extensive mass spectrometer study of the afterglow ion currents would answer several questions, but one must be careful in such measurements, since the binding energy of N_4^+ is low and dissociation through collisions may take place easily in a mass spectrometer system.[52]

The ambipolar diffusion coefficient obtained by the microwave transmission technique has not been previously reported. As mentioned in the results section, $D_a p$ was found to be 123 cm^2 Torr sec^{-1} with a spread of $\pm$ 24 cm^2 Torr sec^{-1}. The ion mobility may be calculated from this value using equation 19. The mobility may be compared with the results of other determinations if it is referred to the normal temperature and pressure values of 0° C. and 760 Torr. This may be done by the formula

$$\mu_o = \frac{7.63\, D_a p_o}{T_g} \qquad \frac{cm/sec}{volt/cm}$$

where $D_a p_o$ is in cm^2 sec^{-1} Torr and T_g is the gas temperature, 300° K in this case. The resultant mobility is 2.85 cm^2 sec^{-1} $volt^{-1}$. This value compares favorably with 2.9 obtained by Tyndall and Pearce[53] in 1935 by drift tube measurements. Faire and Champion[28] deduced a mobility at standard conditions of 2.8 cm^2 sec^{-1} $volt^{-1}$ from measurements of the ambipolar diffusion coefficient, employing the microwave cavity technique.

These results, all in good agreement, raise a perplexing question, however. The mobility of N_2^+ in nitrogen would be expected to show effects of charge transfer[7]. Results of Mitchell and Ridler[46] for mobilities of various gases in nitrogen in which charge transfer would <u>not</u> be expected are shown in Figure 30. From theory[19] one would expect that the mobility in such a situation would be nearly proportional to $(1 + M_g/M_i)^{1/2}$. M_g is the mass of the nitrogen molecule and M_i is the mass of the ion. This trend is evident in Figure 30. However, it is also noted that the value obtained in the present work falls on the curve. The effect of charge transfer has been observed

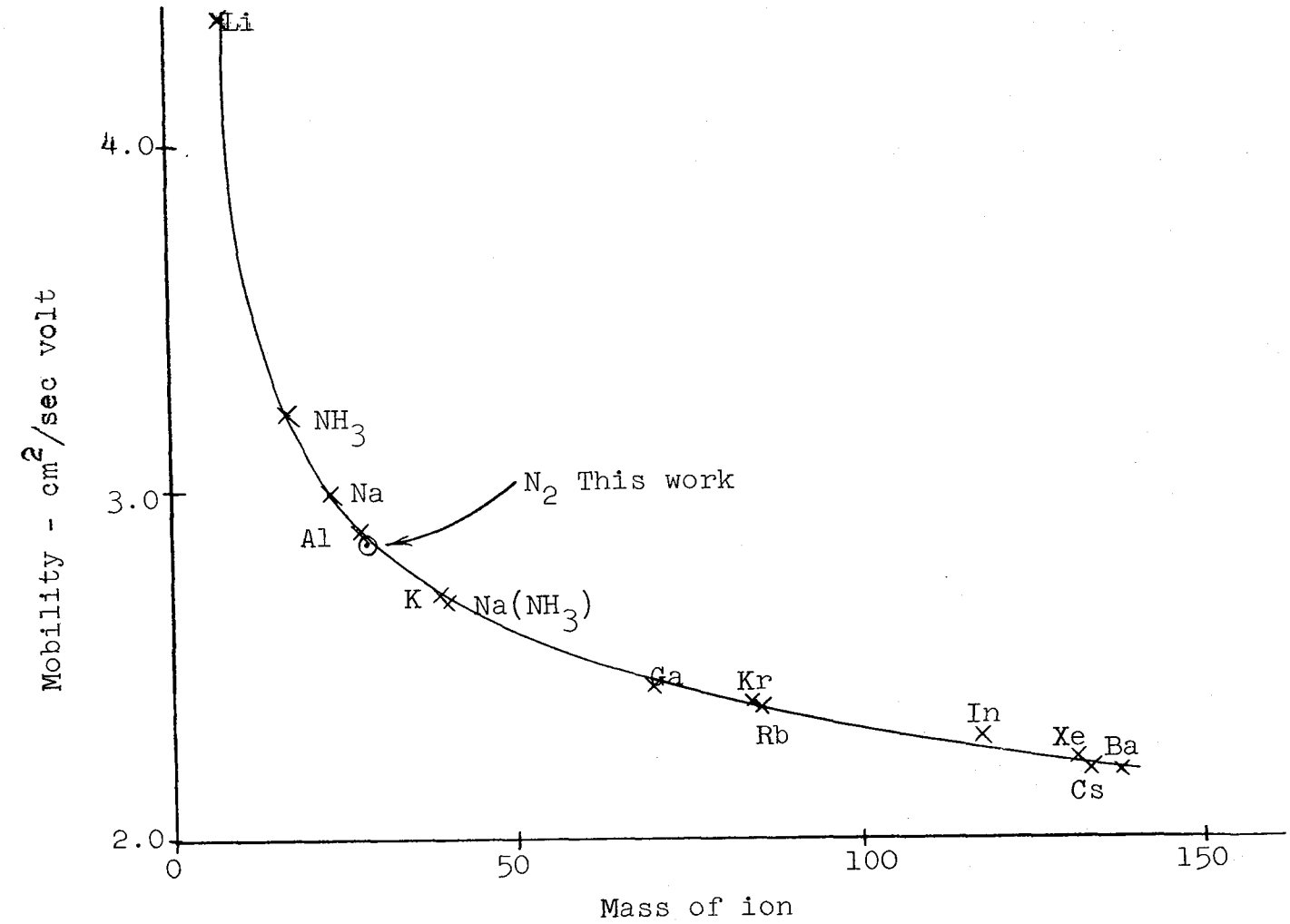

Fig. 30. Mobility in nitrogen of various ions as a function of mass at 1 atmosphere pressure.

in rare gas ions diffusing in their parent gases in the following way.[43] Mobilities of alkali ions in the inert gases were obtained. A plot of mobilities vs. mass of ions similar to Figure 30 was plotted, but it was found in all cases that the point corresponding to the inert gas ion would fall at a point 20 to 60% below the curve. This decrease in mobility was attributed to charge transfer. The theory for the charge exchange effect is not well understood, but some attempts have been made to study this effect in helium[43]. From results of the present measurements it would appear that either charge exchange effects are not as important in the case of molecular ions, or that another process may speed up the diffusion, compensating for the decrease by charge exchange.

The results of the temperature measurements are interesting in that they reveal a source of energy in the early afterglow after the discharge source has been removed. Figure 18 shows the decay of temperature at several different pressures. It is noted that there is a rise in temperature reaching a maximum and then a final decay to room temperature. Not shown in Figure 18 is an initial rapid drop in temperature following the discharge that is difficult to follow because it occurs in a time comparable to the minimum gate width of the microwave radiometer. The point to notice is that the maximum temperature value occurs later in the afterglow at lower pressures.

Two possible explanations of high temperatures in the nitrogen afterglow have been suggested by Formato and Gilardini[29]. First, "some nitrogen molecules are excited to metastable levels during the discharge; metastable-metastable collisions in the afterglow may result in the ionization of one of them, so that a continuous supply of high energy electrons is present in the afterglow". Secondly, "the electron-ion recombination coefficient may decrease with increasing electron energy; low energy electrons are then rapidly removed and the energy distribution is shifted upwards".

The second suggestion seems to be ruled out, since one would expect that this would lead to a monotonically decreasing energy, and could not explain the increase in temperature. The first suggestion

of the presence of metastables appears to be more promising, but even this would require an increase in metastable-metastable collision rate after the discharge source is removed in order to obtain an increase in temperature.

Phelps and Brown[48] have argued that in helium, the electron density actually increases owing to metastable-metastable collisions following high energy discharge pulses through a reaction

$$He^m + He^m \rightarrow He + He^+ + e^-$$

and the related reaction in which a molecular ion is formed

$$He^m + He^m \rightarrow He_2^+ + e^-$$

It is possible, admittedly only through conjecture, that analagous reactions in nitrogen

$$N_2^m + N_2^m \rightarrow N_2 + N_2^+ + e^-$$

$$N_2^m + N_2^m \rightarrow N_4^+ + e^-$$

may cause high energy electrons to appear in the afterglow and to increase the electron temperature. The conjecture is not completely without basis, however. First let us consider a mechanism for increasing the population of metastables following the discharge.

The equations describing the rate of change of the metastable density, M, and the electron density, n, are

$$\frac{\partial M}{\partial t} = -kM + \gamma(\alpha n^2) - \beta M^2 \qquad (86)$$

and

$$\frac{\partial n}{\partial t} = -\alpha n^2 + \beta M^2 \qquad (87)$$

k is the rate of loss per metastable molecule due to destructive

collisions with neutral molecules in the volume of the gas and also may describe the loss represented by the fundamental diffusion mode. γ is the fraction of metastable molecules formed per recombination event. In equation 87, it is assumed that the loss of electrons is primarily by recombination. βM^2 is the rate of formation of electrons by metastable-metastable collisions. Superelastic collisions between electrons and metastables may also provide energetic electrons in the afterglow. In a weakly ionized gas this effect would be small in comparison to the destruction of metastables by neutral particles.

Assume also that βM^2 is negligible with respect to the rate of destruction, kM, in equation 86. The recombination coefficient decreases rapidly with increasing temperature.[2] Thus the formation term in equation 86 increases during the rapid initial decrease in electron energy in the first few microseconds of the afterglow. This would result in an increase in the metastable density. The metastable-metastable collision process would then have an increasing effect during the early afterglow.

Secondly, the time retardation on the peak temperature with decreasing pressure may be explained as follows. At higher pressures the collision frequency for metastable-molecule collisions would be increased. Thus at lower pressures the destruction of metastable states through neutral collisions would proceed at a slower rate, providing for the longer effect noted in the temperature measurements.

The problem in presenting a quantitative analysis of the metastable effect is that the rate of formation and destruction, and the initial density of metastable molecules are unknown. The temperature dependence of the recombination coefficient is also not precisely known. In reference to equation 87, it is seen that all of these factors would have to be obtained in order to determine if the electron density initially increases.

As a further check on this process, measurements of electron density in the very early afterglow are in progress in an attempt to ascertain if the electron density initially increases.

The results of the preliminary measurements for the cross-

section for momentum transfer were given in Figure 29. Although the results are scattered owing to the inaccuracy of attenuation measurements, it is interesting to compare the results with other determinations. This is best done by calculating the collision probability P_m from the cross-section where

$$P_m p_o = N Q_m$$

The curves shown in the papers of Phelps, Fundingsland and Brown[49] (microwave cavity), Anderson and Goldstein[3] (microwave transmission), and Crompton and Sutton[23] (calculated from measurements of electron diffusion and mobility in dc electric fields) are reproduced in Figure 31, along with the results from the present experiment. It is impossible to assign trends to the results of the present experiment, but, as mentioned in part IV 3, the method, with increased accuracy of attenuation measurements, is expected to resolve this point, especially when combined with the direct measurement of electron energy by the microwave radiometer.

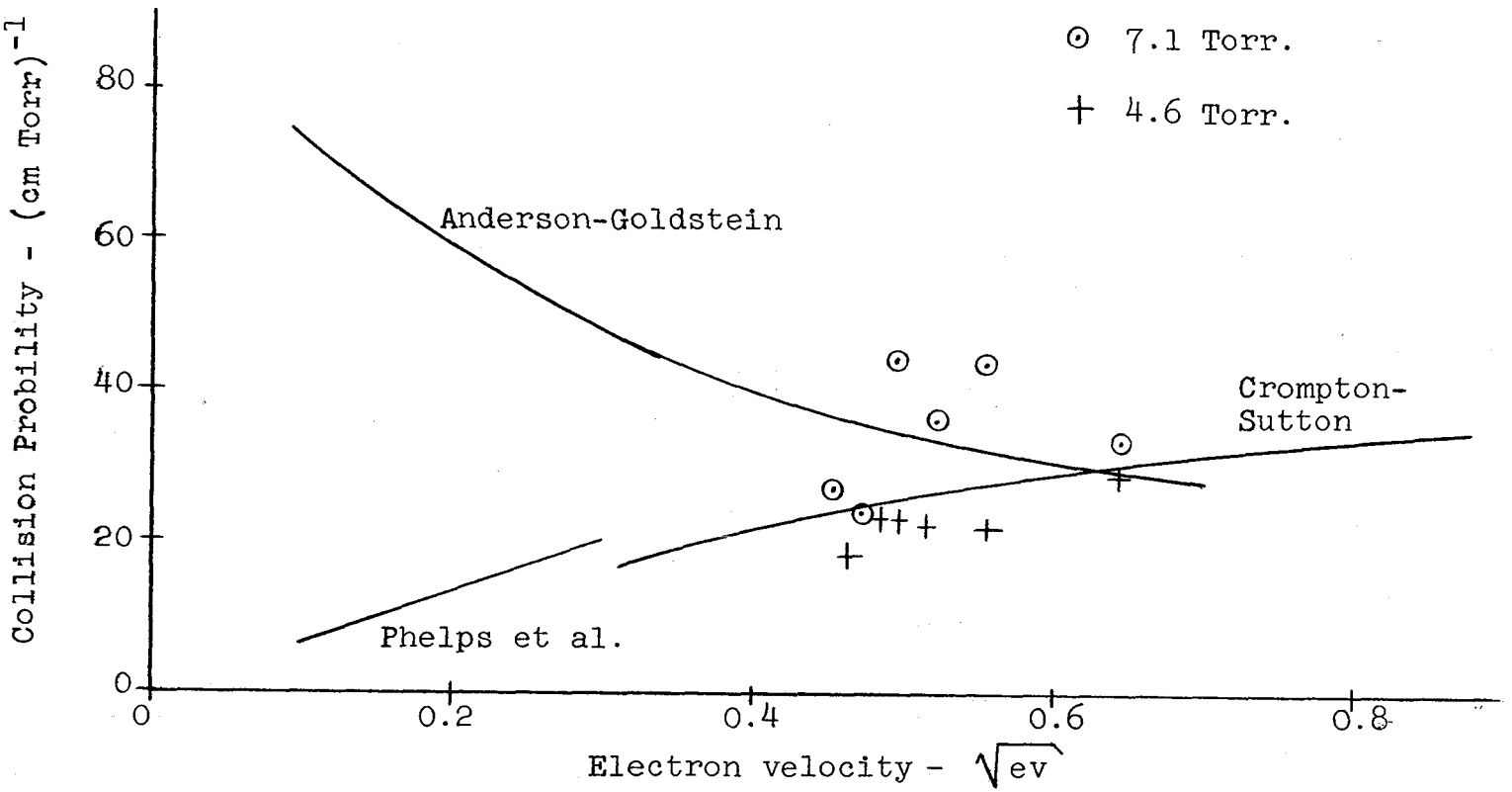

Fig. 31. Collision probability, P_m, vs. electron velocity.

PART VI.

CONCLUSIONS AND SUMMARY

A brief summary of the experimental results is as follows. The room temperature recombination coefficient in the nitrogen afterglow has been measured as 0.4×10^{-7} cm^3/sec at 0.25 Torr rising to 6.8×10^{-7} cm^3/sec at 7.1 Torr. The predominant recombination mechanism is thought to be the dissociative recombination of the N_4^+ molecular ion,

$$N_4^+ + e^- \rightarrow N_2 + N_2^*$$

although the three body reaction

$$N_2^+ + e^- + N_2 \rightarrow N_2 + N_2^*$$

may be a significant process. The ion mobility at standard conditions of 760 Torr, 0^oC, as calculated from the ambipolar diffusion coefficient, is 2.85 cm^2 sec^{-1} $volt^{-1}$, comparing favorably with previous drift tube measurements and microwave cavity measurements. The temperature measurements have indicated a source of energy in the early afterglow which has been attributed to the presence of metastable molecules. Preliminary results for the collision cross-section for momentum transfer are inconclusive, but the problems in the experimental procedure are resolved.

The main conclusion reached is that the afterglow is of such a complexity that a combination of experimental procedures is required to separate and describe the various physical processes which are taking place. The necessity for some of the questionable assumptions used by previous investigators has been eliminated by the determination of the electron temperature by the gated radiometer and the simplification of the geometry for the microwave-plasma interaction. Still unexplained is the apparent absence of charge transfer effects on the mobility. Also the exact recombination mechanism is still unknown. It may be that an intensive study by mass-spectrometer and light spectroscopic techniques will answer some of these questions.

PART VII.

LITERATURE CITED

1. Adler, R. B. Waves on Inhomogeneous Cylindrical Structures. Proc. IRE, 40, part 1, p. 339-348. 1952.

2. Anderson, J. M. and Goldstein, L. Interaction of Electromagnetic Waves of Radio-Frequency in Isothermal Plasmas. Phys. Rev., 100, p. 1037-1046. 1955.

3. Anderson, J. M. and Goldstein, L. Momentum Transfer Cross Section and Fractional Energy Loss in the Collisions of Slow Electrons with Nitrogen Molecules. Phys. Rev., 102, p. 388-389. 1956.

4. Allis, W. P. Motions of Ions and Electrons. Hanbuch der Physik, Vol. 21, p. 396. Springer-Velag, Berlin. 1956.

5. Ibid. p. 404.

6. Bailey, V. A. On the Attachment of Electrons to Gas Molecules. Phil. Mag., 50, p. 825-843. 1925.

7. Bates, D. R. Atomic and Molecular Processes. Academic Press. p. 708. 1962.

8. Bates, D. R. Electron Recombination in Helium. Phys. Rev., 77, p. 718-719. 1950.

9. Bates, D. R. Dissociative Recombination. Phys. Rev., 78, p. 492-493. 1950.

10. Bekefi, G. and Brown, S. C. Microwave Measurements of the Radiation Temperature of Plasmas. J. Appl. Phys., 32, p. 25-30. 1961.

11. Bekefi, G. A Microwave Pyrometer. Quarterly Progress Report No. 57, Research Laboratory of Electronics, MIT, p. 7-11. 1960.

12. Bekefi, G. Emission of Microwaves from Plasmas. Paper given at Rochester Conference on Engineering Aspects of Magnetohydrodynamics. 1962.

13. Bialecki, E. P. and Dougal, A. A. Pressure and Temperature Variation of the Electron-Ion Recombination Coefficient in Nitrogen. J. Geophys. Res., 63, p. 539-546. 1958.

14. Biondi, M. A. and Brown, S. C. Measurements of Ambipolar Diffusion in Helium. Phys. Rev., 75, p. 1700-1705. 1949.

15. Biondi, M. A. and Brown, S. C. Measurement of Electron-Ion Recombination. Phys. Rev., 76, p. 1697-1700. 1949.

16. Boyd, R. L. F. and Morris, D. A Radio-Frequency Probe for the Mass-Spectrometric Analysis of Ion Concentrations. Proc. Phys. Soc.(London), 68A, p. 1-17. 1955.

17. Brown, S. C. Basic Data of Plasma Physics. Wiley, 1959. p. 19.

18. Ibid. p. 23.

19. Ibid. p. 63.

20. Brown, S. C. et. al. Methods of Measuring the Properties of Ionized gases at Microwave Frequencies. Technical Report No. 66 (1948) and No. 140 (1949), Research Laboratory of Electronics, MIT.

21. Bryan, R. B., Holt, R. B. and Oldenberg, O. Recombination and Afterglow in Nitrogen and Oxygen. Phys. Rev., 106, p. 83-86. 1957.

22. Cravath, A. M. The Rate of Formation of Negative Ions by Electron Attachment. Phys. Rev., 33, p. 605-613. 1929.

23. Crompton, R. W. and Sutton, D. J. Experimental Investigation of the diffusion of slow electrons in nitrogen and hydrogen. Proc. Roy. Soc. (London), A215, p. 467-480. 1952.

24. Delcroix, J. L. Introduction to the Theory of Ionized Gases. Interscience, p. 39. 1960.

25. Desloge, E. A., Matthysse, S. W. and Margenau, H. Conductivity of Plasmas to Microwaves. Phys. Rev., 112, p. 1437-1440. 1958.

26. Dicke, R. H. The Measurement of Thermal Radiation at Microwave Frequencies. Rev. of Sci. Inst., 17, p. 268-275. 1946.

27. Dushman, D. Scientific Foundations of Vacuum Technique, 2nd Edition. Wiley, 1962. p. 207.

28. Faire, A. C. and Champion, K. S. W. Measurements of Dissociative Recombination and Diffusion in Nitrogen at Low Pressures. Phys. Rev., 113, p. 1-6. 1959.

29. Formato, D. and Gilardini, A. Microwave Determinations of Afterglow Temperatures and Electron Collision Frequencies in Nitrogen. Fourth Intern. Conf. on Ioniz. Phen. in Gases, p. 99-104, Uppsala, 1959. North Holland Publishing Co., Amsterdam, 1960.

30. Gilardini, A. L. and Brown, S. C. Microwave Conductivity of an Ionized Decaying Plasma at Low Pressures. Phys. Rev., 105, p. 25-30. 1957.

31. Golant, V. E. Microwave Plasma Diagnostic Techniques. Soviet Physics (Technical Physics), 5, p. 1197-1248. 1961.

32. Gray, E. P. and Kerr, D. E. Volume Recombination and Diffusion in Afterglows. Fourth Intern. Conf. on Ioniz. Phen. in Gases, p. 84-88, Uppsala, 1959. North Holland Publishing Co., Amsterdam, 1960.

33. Johnson, R. B., McClure, B. T. and Holt, R. B. Electron Removal in Helium Afterglows. Phys. Rev., 80, p. 376-379. 1950.

34. Kasner, W. H., Rogers, W. A. and Biondi, M. A. Electron-Ion Recombination Coefficients in Nitrogen and in Oxygen. Phys. Rev. Letters, 7, p. 321-323. 1961.

35. Kerr, D. E. and Leffel, C. S. Recombination between Electrons and Helium Molecular Ions. Bull. Amer. Phys. Soc., 42, p. 113. 1959.

36. Loeb, L. B. Basic Processes of Gaseous Electronics. Univ. of California Press, Berkely, 1961.

37. Lozier, W. W. The Heats of Dissociation of Hydrogen and Nitrogen. Phys. Rev., 44, p. 575-581. 1933.

38. Margenau, H. and Stillinger, D. Microwave Conductivity of Slightly Ionized Air. J. of Appl. Phys., 30, p. 1385-1387. 1959.

39. Margenau, H. and Hartman, L. M. Theory of High Frequency Gas Discharges. Phys. Rev., 73, p. 297-328. 1948.

40. Massey, H. S. W. and Burhop, E. H. S. Electronic and Ionic Impact Phenomena. Oxford Press, 1952. p. 6.

41. Ibid. p. 14.

42. Ibid. p. 123.

43. Ibid. p. 409.

44. Ibid. p. 631.

45. Massey, H. S. W. Recombination of Gaseous Ions. Adv. in Phys., 1, p. 395-426. 1952.

46. Mitchell, J. H. and Ridler, K. E. W. The Speed of Positive Ions in Nitrogen. Proc. Roy. Soc.(London), A146, p. 911-921. 1934.

47. Oskam, H. J. Microwave Investigation of Disintegrating Gaseous Discharge Plasmas. Thesis, University of Utrecht, Netherlands. 1957.

48. Phelps, A. V. and Brown, S. C. Positive Ions in the Afterglow of a Low Pressure Helium Discharge. Phys. Rev., 86, p. 102-105. 1952.

49. Phelps, A. V., Fundingsland, O. T. and Brown, S. C. Microwave Determination of the Probability of Collision of Slow Electrons in Gases. Phys. Rev., 84, p. 559-562. 1951.

50. Redfield, A. and Holt, R. B. Electron Removal in Argon Afterglows. Phys. Rev., 82, p. 874-876. 1951.

51. Riesz, R. and Dieke, G. H. The Analysis and Purification of Rare Gases by Means of Electric Discharges. J. Appl. Phys., 25, p. 196-201. 1954.

52. Saporoschenko, M. Ions in Nitrogen. Phys. Rev., 111, p. 1550-1553. 1958.

53. Tyndall, A. M. and Pearce, A. F. The Variation of the Mobility of Gaseous Ions with Temperature. Proc. Roy. Soc.(London), A149, p. 426-434. 1935.

54. Varney, R. N. Drift Velocity of Ions in Oxygen, Nitrogen, and Carbon Monoxide. Phys. Rev., 89, p. 708-711. 1953.

55. Varney, R. N. Drift Velocities of Ions in Nitrogen at Various Temperatures. Phys. Rev., 107, p. 1490-1492. 1957.

56. Whitmer, R. F. Microwave Studies of the Electron Loss Processes in Gaseous Discharges. Phys. Rev., 104, p. 572-575. 1956.

PART VIII.

APPENDIX

Approximations in the Solution of Equation 39, Page 19

Equation 39, page 19, describes the time and spatial variation of the electron density when loss occurs simultaneously by diffusion and recombination.

$$\frac{\partial n}{\partial t} = D_a \nabla^2 n - \alpha n^2 \qquad (39)$$
$$(A1)$$

Unfortunately, no exact solution is known and one is forced to make approximations in order to obtain the coefficients D_a and α. In the late afterglow the usual assumptions made are that αn^2 is small and that the fundamental diffusion mode predominates. Biondi and Brown[14] and Faire and Champion[28] have used an approximating equation

$$\frac{\partial n}{\partial t} = -kn - \alpha n^2 \qquad (A2)$$

where the constant k is the reciprocal of the time constant of the fundamental diffusion mode. In solving equation A2, they assumed n to be spatially independent; hence the partial derivative becomes the total derivative in time.

Redfield and Holt[50] have used an approximation which is derived as follows: the spatial distribution of electrons is assumed to be that of the fundamental diffusion mode. In the rectangular waveguide cell this would be

$$n = n_o(t) \sin\frac{\pi y}{b} \sin\frac{\pi y}{b} \sin\frac{\pi z}{c} \qquad (A3)$$

If the product of the three sine terms is written as m(r) and equation A3 is substituted in A1, the result is

$$\frac{\partial n_o(t)}{\partial t} = -kn_o(t) - \alpha n_o^2(t)\, m(r) \qquad (A4)$$

Equation A4 is then integrated over the volume of the container. In

the waveguide cell the result is

$$\frac{dn_o(t)}{dt} = -kn_o(t) - \frac{8}{\pi^3}\alpha n_o^2(t) \tag{A5}$$

In the approximating equation (equation 40, page 20) used throughout this thesis, the spatial term m(r) in equation A4 was evaluated at the center of the cell where it has the value of unity. This results in the same form of equation as used by Biondi and Brown, and by Faire and Champion, so that comparisons of previous measurements in nitrogen could be made. Note that this would result in a value for the recombination coefficient which differs by a factor of $8/\pi^3$ or 0.258 from the method of approximation by Redfield and Holt. The difference factor, derived in a similar manner, for the two approximations in a cylindrical cavity is 0.275.

The approximate solution used in this thesis (equation 42) is

$$n_o(t) = \frac{C_1 k e^{-kt}}{1 - \alpha C_1 e^{-kt}} \tag{A6}$$

Some idea of the error involved may be found by substituting this solution into the original equation A1. If equation A1 is written in the form

$$E = \frac{\partial n}{\partial t} - D_a \nabla^2 n + \alpha n^2 \tag{A7}$$

E is zero for an exact solution. Now if equations A3 and A6 are substituted into equation A7, the time and spatial variation of the error expression, E, is

$$E = \frac{m(r)\alpha C_1^2 k^2 e^{-2kt}}{(1 - \alpha C_1 e^{-kt})^2} \left(m(r) - 1 \right) \tag{A8}$$

where $m(r) = \sin\frac{\pi x}{a} \sin\frac{\pi y}{b} \sin\frac{\pi z}{c}$

Since the error is a function of the spatial variables, the original assumption of the sinusoidal spatial variation is, of course, wrong. Note that E is zero at the center of the cell and at the cell boundaries, the latter being trivial since n is zero at the boundaries for all time. Since E decreases with time at all spatial positions, the distribution approaches one which is sinusoidal. The exponential rate is essentially twice the rate of the fundamental diffusion mode.

Rennselaer Polytechnic Institute,
Troy, New York.

NASA-Langley, 1963 D-2226